Self-similar polytropic champagne flows in H II regions

Ren-Yu Hu[1]★ and Yu-Qing Lou[1,2,3]★

[1]*Physics Department and Tsinghua Centre for Astrophysics (THCA), Tsinghua University, Beijing 100084, China*
[2]*Department of Astronomy and Astrophysics, The University of Chicago, 5640 South Ellis Avenue, Chicago, IL 60637, USA*
[3]*National Astronomical Observatories, Chinese Academy of Science, A20 Datun Road, Beijing 100012, China*

ABSTRACT

We explore large-scale hydrodynamics of H II regions for various self-similar shock flows of a polytropic gas cloud under self-gravity and with quasi-spherical symmetry. We formulate cloud dynamics by invoking specific entropy conservation along streamlines and obtain global self-similar 'champagne flows' for a conventional polytropic gas with shocks as a subclass. Molecular cloud cores are ionized and heated to high temperatures after the onset of nuclear burning of a central protostar. We model subsequent evolutionary processes in several ways and construct possible self-similar shock flow solutions. We may neglect the mass and gravity of the central protostar. The ionization and heating of the surrounding medium drive outflows in the inner cloud core and a shock travels outwards, leading to the so-called 'champagne phase' with an expanding outer cloud envelope. Complementarily, we also consider the expansion of a central cavity around the centre. As the inner cloud expands plausibly due to powerful stellar winds, a cavity (i.e. 'void' or 'bubble') can be created around the centre, and when the cavity becomes sufficiently large, one may neglect the gravity of the central protostar. We thus present self-similar shock solutions for 'champagne flows' with an expanding central void. We compare our solutions with isothermal solutions and find that the generalization to the polytropic regime brings about significant differences of the gas dynamics, especially for cases of $n < 1$, where n is a key scaling index in the self-similar transformation. We also compare our global polytropic self-similar solutions with numerical simulations on the expansion of H II regions. We further explore other possible dynamic evolutions of H II regions after the initiation of nuclear burning of the central protostar, for example asymptotic inflows or contractions far from the cloud centre and the ongoing infall around a central protostar. In particular, it is possible to use the downstream free-fall solution with shocks to describe the dynamic evolution of H II regions shortly after the nascence of the central protostar. We also give an analysis on the invariant form of self-similar polytropic flows by ignoring self-gravity.

Key words: hydrodynamics – shock waves – stars: formation – stars: winds, outflows – ISM: clouds – H II regions.

1 INTRODUCTION

The compact (scale sizes of $\sim$0.1–1 pc) and ultracompact (UC; scale sizes $\lesssim$0.15 pc) H II regions are associated with massive OB stars (e.g. Habing & Israel 1979). The UC H II region stage ($\lesssim$10^5 yr) stands for a substantial part of the relatively short main-sequence lifetimes of OB stars. Several radio surveys (e.g. Wood & Churchwell 1989; Fish 1993; Kurtz, Churchwell & Wood 1994) observed expansions of luminous H II regions with shock signatures. 'champagne flow' models (e.g. Tenorio-Tagle 1979; Tenorio-Tagle, Yorke & Bodenheimer 1979; Yorke 1986) successfully explain the expansion of H II regions by considering a protostar formed in a

cloud core, photoionizing and heating the cloud, as well as driving a shock that accelerates the ionized gas to expand rapidly. Observations tend to support 'champagne flow' models, such as Lumsden & Hoare (1999) for UC H II regions G29.96−0.02 and Barriault & Joncas (2007) for compact H II region Sh 2−158. Champagne flows in clouds of larger scales have also been identified, such as Foster et al. (2007) for the dense Galactic H II region G84.9+0.5 and Maheswar et al. (2007) for the classical H II region S236 in the cluster of OB stars NGC 1893.

Tenorio-Tagle (1979) classified champagne flows into cases R and D. For the case R, the ionization front (IF) created by the emergence of the central massive protostar rapidly breaks out from the dense cloud and leaves the gas behind it fully ionized. For the case D, the IF is 'trapped' inside a cloud, and produces an expanding H II region within a cloud. In the formation phase of

★E-mail: hu-ry07@mails.tsinghua.edu.cn (R-YH); louyq@tsinghua.edu.cn (Y-QL)

H II regions, whether the IF is R type or D type depends on the initial grain opacity, the ionizing flux and the initial density and the size of a cloud (Franco, Tenorio-Tagle & Bodenheimer 1990). In the expansion phase, H II regions with an initial mass density profile $\rho \propto r^{-l}$ and $l > 3/2$ are 'density bounded', where ρ is the mass density and r is the radius (see e.g. Osterbrock 1989; Franco et al. 1990).[1] It is also possible that the D-type IF changes to a weak R-type IF when $l > 3/2$. In such cases, the fully ionized cloud begins to expand and an outgoing shock forms. This is referred to as the 'champagne phase' (Bodenheimer, Tenorio-Tagle & Yorke 1979). Notably if a shock front encounters a steep negative density gradient, for example, the edge of a cloud, asymmetric 'champagne flows' may occur, as observed by Lumsden & Hoare (1999). According to the Very Large Array (VLA) survey by Wood & Churchwell (1989), 16 per cent of H II regions bear cometary appearance. Arthur & Hoare (2006) numerically simulated 'cometary champagne flows'. If $l < 3/2$, the H II region is 'ionization bounded', e.g. the ultraviolet (UV) radiation is trapped within a finite radius (Osterbrock 1989). In such cases, the ionized region should expand as $t^{4/(7-2l)}$, driving a shock that would accelerate the ambient medium into a thin shell (Franco et al. 1990). In this paper, we focus on the champagne phase of a cloud assumed to be 'density bounded', implying $l > 3/2$. We also assume that the cloud is fully ionized shortly after the onset of nuclear burning of a central massive protostar.

Shu et al. (2002) (also Tsai & Hsu 1995) investigated isothermal 'champagne flows' under spherical symmetry in the self-similar framework. By neglecting the gravity of the central massive protostar and assuming that a cloud initially stays at rest and gets heated by the luminous massive protostar to a uniform high temperature, one may obtain self-similar expansion solutions connected with isothermal outflows with shocks; this corresponds to a 'champagne flow' in a highly idealized setting. The initial isothermal mass density profile scales as $\rho \propto r^{-2}$. In addition, for molecular clouds with other possible initial mass density profiles, Shu et al. (2002) also ignored the self-gravity of a cloud completely and proposed another self-similar transformation, referred to as the 'invariant form', and obtained solutions for cases with an initial mass density profile $\rho \propto r^{-l}$, where the power-law index l is not necessarily equal to 2. In general, it is not realistic to suppose molecular clouds to be isothermal in many astrophysical situations. One specific example of cloud temperature measurement of a UC H II region NGC 6334F undergoing a 'champagne flow' reveals a conspicuous temperature gradient from the centre to the edge (e.g. De Buizer et al. 2002).

Energy sources and plasma coolings in molecular clouds are not completely known. We then approximate the energy equation by a general polytropic equation of state $p = \kappa(r, t) \, \rho^{\gamma}$, where p is the thermal gas pressure, γ is the polytropic index and the proportional coefficient $\kappa(r, t)$ (related to the specific entropy) depends on radius r and time t in general. Setting κ as a global constant, the equation of state simply becomes a conventional polytropic one. By adjusting γ, we may model various situations of H II regions in molecular clouds. For example, for $\gamma = 1$ and a constant κ, our solutions reduce to isothermal ones. Since 'champagne flows' in a polytropic molecular cloud has not been studied, we would generalize the isothermal analyses of Tsai & Hsu (1995) and of Shu et al. (2002) to a polytropic description of self-similar 'champagne flows'. We shall provide the basic formulation with the most general polytropic equation of state (i.e. specific entropy conservation along streamlines; Wang &

Shu et al. (2002) introduced the Bondi–Parker radius as a measure for the effective distance of the central gravity. The Bondi–Parker radius is defined by $r_{BP} = GM_*/(2a^2)$, where M_* is the mass of the central gravity source and a is the sound speed of the surrounding medium, which is a constant for an isothermal cloud. The mass originally residing within a radius r_0 is dumped into the star during the star formation. After the star formation, as the surrounding cloud becomes much hotter with a higher sound speed, the Bondi–Parker radius becomes much less than r_0. Therefore for the gas in $r > r_0$, the gravity of the central massive star may be neglected. This reasoning naturally leads to the possible existence of a cavity around the centre of a molecular cloud, which we refer to as 'void' or 'bubble'. At $t = 0$, the void boundary is at $r = r_0$. For an expanding cloud, the central void also expands. Indeed, a stellar wind drives also a principal shock and is capable of sweeping the surrounding ionized gas into an expanding shell. Wood & Churchwell (1989) identified central cavities in the shell or cometary UC H II regions, which are thought to be supported by stellar winds and radiation pressures in their survey. Lumsden & Hoare (1999) suggested a 'champagne flow' surrounding a hot stellar wind bubble to interpret observations of G29.96−0.02. Comerón (1997) numerically simulated the dynamic evolution of wind-driven H II regions with strong density gradients and found that features of classical champagne model are not substantially changed, except that the compression of the swept-up matter would, rapidly and particularly in densest cases, lead to the trapping of the IF and inhibit the champagne phase. Therefore, the dynamic evolution of void expansion represents an important physical aspect of 'champagne flows'. Chevalier (1997) studied the isothermal self-similar evolution of the planetary nebulae with the consideration of fast winds blowing off the slow winds. The contact discontinuity between the fast winds and the slow winds suggested by Chevalier (1997) corresponds to the concept of void boundary of this work. Recently, Lou & Hu (2008) explore self-similar solutions for voids in a more general context. In this paper, we construct self-similar solutions for 'champagne flows' with central voids in self-similar expansion. The inclusion of a central void not only makes our polytropic model more realistic, but also allows us to take into account stellar wind bubbles.

We outline the model formulation of a general polytropic gas and present self-similar asymptotic solutions in Section 2 and construct global solutions of 'champagne flows' in Section 3. Section 4 provides solutions of self-similar 'champagne flows' with an expanding central void. In section 5, we discuss behaviours and astrophysical applications of our novel solutions, and suggest other plausible forms of H II regions. Details of an invariant form of self-similar solutions in a conventional polytropic gas with the self-gravity ignored are summarized in Appendix A.

2 SELF-SIMILAR POLYTROPIC FLOWS

2.1 General polytropic formulation

Dynamic evolution of a quasi-spherical general polytropic gas under self-gravity can be described by non-linear hydrodynamic equations in spherical polar coordinates (r, θ, ϕ):

$$\frac{\partial \rho}{\partial t} + \frac{1}{r^2} \frac{\partial}{\partial r}(r^2 \rho u) = 0, \tag{1}$$

$$\frac{\partial M}{\partial t} + u \frac{\partial M}{\partial r} = 0, \tag{2}$$

$$\frac{\partial M}{\partial r} = 4\pi r^2 \rho, \tag{3}$$

$$\rho\left(\frac{\partial u}{\partial t} + u\frac{\partial u}{\partial r}\right) = -\frac{\partial p}{\partial r} - \frac{GM\rho}{r^2}, \tag{4}$$

$$p = \kappa(r, t)\rho^\gamma, \tag{5}$$

where $\rho(r, t)$ is the mass density, $u(r, t)$ is the bulk gas radial flow velocity, $M(r, t)$ is the enclosed mass within r at time t, p is the thermal pressure, $G = 6.67 \times 10^{-8}$ dyne cm^2 g^{-2} is the gravity constant. Equations (1)–(3) describe the mass conservation, equation (4) is the radial momentum equation and equation (5) is the general polytropic equation of state, in which γ is the polytropic index and the coefficient κ directly related to the 'specific entropy' depends on r and t. For a conventional polytropic gas, κ is a global constant in space and time. More generally, we require the conservation of 'specific entropy' along streamlines, namely

$$\left(\frac{\partial}{\partial t} + u\frac{\partial}{\partial r}\right)\left(\ln\frac{p}{\rho^\gamma}\right) = 0. \tag{6}$$

This set of equations is the same as those of Wang & Lou (2008) but without a completely random magnetic field. We should require $\gamma > 1$ to ensure the positiveness of the gas enthalpy.

To reduce the non-linear partial differential equations (PDEs) to ordinary differential equations (ODEs) for self-similar flows, we introduce the following transformation:

$$r = k^{1/2}t^n x, \qquad u = k^{1/2}t^{n-1}v, \qquad \rho = \frac{\alpha}{4\pi G t^2},$$

$$p = \frac{kt^{2n-4}}{4\pi G}\beta, \qquad M = \frac{k^{3/2}t^{3n-2}m}{(3n-2)G}, \tag{7}$$

where x is a dimensionless independent self-similar variable, k is a dimensional parameter related to the polytropic sound speed making x dimensionless, $v(x), \alpha(x), \beta(x), m(x)$ are dimensionless reduced dependent variables of x only and n is a key scaling index which controls the relation between r and x as well as various scalings of reduced dependent variables. We will see in the following that n scales the initial density profile of the gas. We refer to $v(x), \alpha(x), \beta(x)$ and $m(x)$ as the reduced radial flow speed, mass density, thermal pressure and enclosed mass, respectively. Transformation (7) is identical with that of Lou & Wang (2006).

By performing self-similar transformation (7) in equations (1)–(6) and introducing parameter $q \equiv 2(n + \gamma - 2)/(3n - 2)$, we obtain two integral relations:

$$m = \alpha x^2(nx - v), \tag{8}$$

$$\beta = \alpha^\gamma m^q, \tag{9}$$

where there is no loss of generality to set the proportional coefficient (i.e. an integration constant) equal to unity in integral (9) for $q \neq 2/3$ or $\gamma \neq 4/3$ (Wang & Lou 2008). The special case of $\gamma = 4/3$ corresponds to a relativistically hot gas as studied by Goldreich & Weber (1980) and Lou & Cao (2008). By setting $q = 0$, the general polytropic formulation reduces to the conventional polytropic case of a global constant κ (e.g. Suto & Silk 1988; Lou & Gao 2006; Lou & Wang 2006; Lou, Jiang & Jin 2008) with $n + \gamma = 2$. According to expression $M(r, t)$ for the enclosed mass in transformation (7), we require $3n - 2 > 0$ and $nx - v > 0$ to ensure a positive enclosed mass. The inequality $3n - 2 > 0$ will re-appear later for a class of asymptotic solutions at large x. By equation (8), we emphasize that for $nx - v = 0$ at a certain x^*, the enclosed mass within x^* becomes zero; we refer to this as a central void and x^* is the independent similarity variable marking the void boundary which expands with time t in a self-similar manner. The relation $v = nx$ shows the speed of the void boundary is the same as the speed of the gas on the void boundary, e.g. the contact discontinuity (Chevalier 1997).

Combining all reduced equations above, we readily derive two coupled non-linear ODEs for α' and v' as

$$\mathcal{X}(x, \alpha, v)\alpha' = \mathcal{A}(x, \alpha, v), \quad \mathcal{X}(x, \alpha, v)v' = \mathcal{V}(x, \alpha, v), \tag{10}$$

where functionals $\mathcal{X}$, $\mathcal{A}$ and $\mathcal{V}$ are defined by

$$\mathcal{X}(x, \alpha, v) \equiv [2 - n + (3n - 2)q/2]\alpha^{1-n+3nq/2}$$
$$\times x^{2q}(nx - v)^q - (nx - v)^2,$$

$$\mathcal{A}(x, \alpha, v) \equiv 2\frac{x - v}{x}\alpha\left[q\alpha^{1-n+3nq/2}x^{2q}(nx - v)^{q-1}\right.$$
$$+ (nx - v)\Big] - \alpha\left[(n - 1)v + \frac{nx - v}{3n - 2}\alpha\right.$$
$$+ q\alpha^{1-n+3nq/2}x^{2q-1}(nx - v)^{q-1}(3nx - 2v)\Big],$$

$$\mathcal{V}(x, \alpha, v) \equiv 2\frac{x - v}{x}\alpha\left(2 - n + \frac{3n}{2}q\right)\alpha^{-n+3nq/2}x^{2q}$$
$$\times (nx - v)^q - (nx - v)\left[(n - 1)v + \frac{nx - v}{3n - 2}\alpha\right.$$
$$+ q\alpha^{1-n+3nq/2}x^{2q-1}(nx - v)^{q-1}(3nx - 2v)\Big]. \tag{11}$$

For a conventional polytropic gas of constant κ with $n + \gamma = 2$, we simply set $q = 0$ in equation (11) to derive

$$\frac{\alpha'}{\alpha^2} = \frac{(n - 1)v + [(nx - v)\alpha/(3n - 2)] - 2(x - v)(nx - v)/x}{\alpha(nx - v)^2 - \gamma\alpha^\gamma}, \tag{12}$$

$$v' = $$
$$\frac{(n - 1)\alpha v(nx - v) + [(nx - v)^2/(3n - 2)]\alpha^2 - 2\gamma\alpha^\gamma(x - v)/x}{\alpha(nx - v)^2 - \gamma\alpha^\gamma}. \tag{13}$$

Up to this point, our basic self-similar hydrodynamic formulation is the same as that of Lou & Wang (2006) and of Wang & Lou (2008) without a random magnetic field.

For energy conservation, we define the energy density ϵ and the energy flux density $\mathcal{J}$ as follows:

$$\epsilon = \frac{\rho u^2}{2} - \frac{GM\rho}{r} + \frac{i}{2}p, \tag{14}$$

$$\mathcal{J} = \rho u\left(\frac{u^2}{2} - \frac{GM}{r} + \frac{i}{2}\frac{\gamma p}{\rho}\right), \tag{15}$$

where ϵ is the energy density, $\mathcal{J}$ is the energy flux density and i is the degree of freedom of an individual gas particle. The three terms in expressions (14) and (15) correspond to densities of the kinetic energy, the gravitational energy and the internal energy, respectively. With equations (1)–(5) and a globally constant κ, we derive

$$\frac{\partial \epsilon}{\partial t} + \frac{1}{r^2}\frac{\partial}{\partial r}(r^2\mathcal{J}) = \mathcal{P} \equiv u\frac{\partial p}{\partial r}\left[\frac{i}{2}(\gamma - 1) - 1\right] \tag{16}$$

for energy conservation, where $\mathcal{P}$ represents the net energy input. If the gas expands adiabatically or $\gamma = (i + 2)/i$, then $\mathcal{P} = 0$. Whether the gas locally gains or loses energy depends not only on the difference between γ and $(i + 2)/i$, but also on the signs of $\partial p/\partial r$ and u.

2.2 Self-similar solutions

An exact globally static solution known as the singular polytropic sphere (SPS) takes the following form of

$$v = 0, \quad \alpha = \left[\frac{n^{2-q}}{2(2-n)(3n-2)} \right]^{-1/(n-3nq/2)} x^{-2/n}. \quad (17)$$

This is a straightforward generalization of the singular isothermal sphere (SIS; e.g. Shu 1977) and of the SPS for a conventional polytropic gas with $q = 0$ (Lou & Gao 2006; Lou & Wang 2006). For a general SPS here, the mass density profile scales as $\rho \propto r^{-2/n}$, independent of q parameter.

For large x, the asymptotic flow behaviour is

$$v = \left[-\frac{nA}{(3n-2)} + 2(2-n)n^{q-1}A^{1-n+3nq/2} \right] x^{1-2/n}$$
$$+ Bx^{1-1/n} + \cdots, \quad (18)$$

$$\alpha = Ax^{-2/n} + \cdots, \quad (19)$$

where $A > 0$ and B are two constant parameters. As $x \to +\infty$, the mass density profile scales the same way as SPS (17) above, independent of q parameter to the leading order. Since $x \to +\infty$ means $t \to 0^+$, the asymptotic solution at large x is thus equivalent to initial conditions of the system at a finite r. Coefficients A and B are referred to as the mass and velocity parameters, respectively. A global solution with asymptotic behaviour (18) and (19) represents a fluid whose density profile scales initially similar to that of a SPS. Thus, by varying the scaling index n or the polytropic index γ, we are able to model the initial density profile with an index $l = -2/n$. Furthermore, as a physical requirement for plausible similarity solutions of our polytropic flow, both $v(x)$ and $\alpha(x)$ should remain finite or tend to zero at large x. Hence, in cases of $2/3 < n < 1$, corresponding to $2 < l < 3$, A and B are fairly arbitrary, while in cases of $1 \leqslant n < 2$ (general polytropic), corresponding to $1 < l \leqslant 2$, B should vanish for a finite radial flow velocity at large x.

In the regime of $x \to 0^+$, there exists a free-fall asymptotic solutions for which the gravity is virtually the only force in action, and the radial velocity and the mass density profile both diverge in the limit of $x \to 0^+$. To the leading order, the free-fall asymptotic solution takes the form of

$$\alpha(x) = \left[\frac{(3n-2)m(0)}{2x^3} \right]^{1/2}, \quad (20)$$

$$v(x) = -\left[\frac{2m(0)}{(3n-2)x} \right]^{1/2}, \quad (21)$$

where constant $m(0)$ represents an increasing central point mass. Such solutions were first found by Shu (1977) in the isothermal case, and were generalized to the conventional polytropic case (Cheng 1978; Lou & Gao 2006; Lou & Wang 2006) and to the general polytropic case with a random magnetic field by Wang & Lou (2008). The asymptotic form does not depend on q. The validity of such solutions requires $n > 2/3$ and $\gamma < 5/3$; the last inequality appears as a result of comparing various terms in series expansions.

Another exact global solution, known as the Einstein–de Sitter (EdS) solution, exists in two cases of $q = 0$ and $q = 2/3$. The EdS solution for a conventional polytropic gas of $q = 0$ reads as

$$v = \frac{2}{3}x, \qquad \alpha = \frac{2}{3}, \qquad m = \frac{2(n-2/3)}{3}x^3 \quad (22)$$

(Lou & Wang 2006); for $q = 2/3$ and thus $\gamma = 4/3$, this global EdS solution without and with a random magnetic field takes a slightly different form (Lou & Cao 2008). With shocks, EdS solutions can be used to construct polytropic 'champagne flows' with various upstream dynamic behaviours.

From now on, we focus on the conventional polytropic case of $q = 0$ with $n + \gamma = 2$. To simulate 'champagne flows' in H II regions in star-forming clouds, we solve coupled non-linear ODEs (12) and (13) subject to the inner boundary conditions at $x = 0$, namely,

$$\alpha = \alpha_0, \qquad v = 0, \quad (23)$$

where α_0 is a constant. A series expansion yields the Larson–Penston (LP) type of asymptotic solutions at small x in the form of

$$v = \frac{2}{3}x - \frac{\alpha_0^{(1-\gamma)}}{15\gamma} \left(\alpha_0 - \frac{2}{3} \right) \left(n - \frac{2}{3} \right) x^3 + \cdots, \quad (24)$$

$$\alpha = \alpha_0 - \frac{\alpha_0^{(2-\gamma)}}{6\gamma} \left(\alpha_0 - \frac{2}{3} \right) x^2 + \cdots. \quad (25)$$

The isothermal counterpart of this polytropic series solution was obtained earlier (Larson 1969a,b; Penston 1969a,b; Hunter 1977; Shu et al. 2002) with $n = 1$ and $\gamma = 1$. Such LP-type solutions may be utilized to construct champagne flows, if we ignore the central protostar as an approximation and assume the surrounding gas to be initially static (e.g. Shu et al. 2002). Physically, as a result of the gravity of the central protostar, the gas infall towards the very central region may not stop, even when the protostar starts to shine and the 'champagne phase expansion' has occurred in the outer cloud envelope due to the photoionization and UV heating. Thus with central free falls (20) and (21) as the downstream side of a shock, we can also construct global solutions for the dynamics of H II regions surrounding a nascent central massive protostar which involves free-fall materials. We can take LP-type or EdS solutions as the downstream side of a shock and model classical champagne flows for a conventional polytropic gas. We shall come to the possible scenario of inner free-fall solutions with an outer champagne flow.

With the restriction $n + \gamma = 2$ for a conventional polytropic gas, the initial density profile with the scaling index n is directly linked to the polytropic index γ, depending on the energy exchange process in the gas (see equation 16). For a general polytropic gas with $q \neq 0$ in contrast, the scaling index n and polytropic index γ can be independently specified; in particular, we can have $\gamma > 1$ and $n \geq 1$ (this is impossible for a conventional polytropic gas). On the other hand, the initial mass density profile is affected by the star formation or other energetic processes before $t = 0$. Hence for $l = -2/n$, we postulate that the energy exchange process remains largely unchanged after the protostar formation at $t = 0$. This is plausible because the IF travels relatively fast to large distances in a cloud during the 'champagne flow' phase. Our general polytropic model allows inequality $2/3 < n < 2$, corresponding to $1 < l < 3$, which covers so far the entire range of initial mass density profiles of H II regions. This range of mass density distribution has been obtained from radio observations of cloud fragments and isolated dark clouds (e.g. Arquilla & Goldsmith 1985; Myers 1985).

Franco et al. (1990) reveals that the initial mass density profile index $3/2 < l < 3$ (i.e. $2/3 < n < 4/3$ in a polytropic model) leads to 'champagne flows' in clouds with weak shocks; and $l > 3$ corresponds to a 'champagne flow' with strong and accelerating shocks. We then require parameter n within the range $2/3 < n$

< 4/3, as we assume the cloud is 'density bounded'. With such range of parameter, we provide solutions of 'champagne flow' with shocks. We emphasize in particular that there is one more degree of freedom to choose the velocity parameter B in asymptotic solution (18) and (19) in polytropic cases with $2/3 < n < 1$ (i.e. $2 < l < 3$) than in the isothermal case. This leads to major differences of the polytropic champagne flow solutions we find as compared with those isothermal solutions of Tsai & Hsu (1995) and Shu et al. (2002). Franco et al. (2000) have recently argued from the radio continuum spectra that UC H II regions have initial density gradients with $2 \leqslant l \leqslant 3$; so we would consider primarily the n range of $2/3 < n < 1$ or $2 < l < 3$. In summary, molecular clouds with $3/2 < l < 3$ have 'champagne flows' in self-similar manner, while those clouds with $l \geqslant 3$ have 'champagne flows' without similarity. For clouds with $2 < l < 3$, there is more than one parameter to specify initial dynamic flows.

Finally, we need to include shocks at proper places in LP-type solutions, EdS solutions or free-fall solutions to match with appropriate asymptotic solutions at large x to determine relevant coefficients. The shock jump conditions between the downstream and upstream variables are determined by the mass conservation, the radial momentum conservation and the energy conservation. With these three equations for shock conditions, one can determine upstream self-similar variables (x_{su}, α_u, v_u) uniquely from downstream self-similar variables (x_{sd}, α_d, v_d) or vice versa. The two subscripts d and u here denote the downstream and upstream variables, respectively. Detailed formulation and procedure of self-similar shocks can be found in section 5 of Lou & Wang (2006). All solutions in this paper are obtained by solving coupled non-linear ODEs (12) and (13) for a conventional polytropic gas with $n + \gamma = 2$.

3 POLYTROPIC CHAMPAGNE FLOWS

In cases of $n < 1$, there is a range of shock positions (or speeds) for a specified downstream solution with a fixed density at the centre α_0 at $x = 0$, corresponding to different asymptotic flow behaviours at large x on the upstream side. We now discuss two situations: first, for cases with a fixed value of α_0, we adjust shock positions for a specified LP-type solution and observe the relation between shock positions and asymptotic flow behaviours at large x. Secondly, for cases with a fixed shock position, we alter the value of α_0 and examine the variation of upstream conditions. It is expected to set certain limits on relevant parameters for polytropic 'champagne flows' to exist. As a series of examples, we choose the scaling index $n = 0.9$. Numerical explorations have also been performed for cases of $n = 0.7$ and 0.8 and the results are qualitatively similar.

3.1 Cases with a fixed α_0 value

With a fixed value of α_0 for $x \rightarrow 0^+$, one can uniquely determine a LP-type solution by a standard numerical integration. Such a LP-type solution will encounter the sonic critical curve at a certain x_{max} uniquely corresponding to α_0. It is natural to consider possible hydrodynamic shock positions $x_{sd} < x_{max}$ on the downstream side of shock front. One such example of $n = 0.9$ and $\alpha_0 = 1$ is shown in Fig. 1 with relevant parameters summarized in Table 1. To model 'champagne flows' with outward expansions at large radii in molecular clouds, we provide the following analysis. In principle, there are two other conditions giving rise to two minima of x_{sd} in order to obtain an outflow in the upstream side of a shock. First, our extensive numerical explorations reveal that there exists a x_{min1} and for $x_{sd} < x_{min1}$, the upstream shock position x_{su} becomes complex
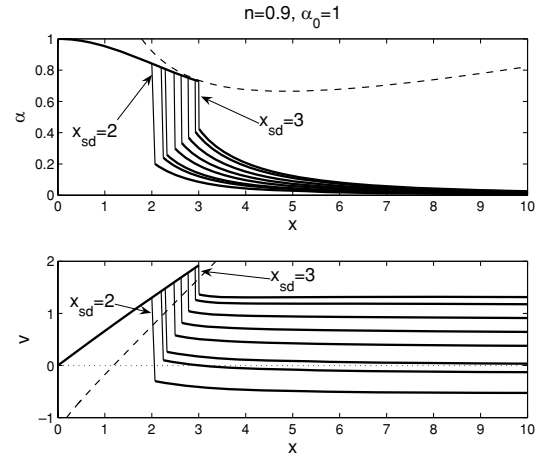
Figure 1. The reduced mass density $\alpha(x)$ (top) and the reduced radial flow velocity $v(x)$ (bottom) for global 'champagne flow' solutions in cases with $n = 0.9$ (thus $\gamma = 1.1$) and $\alpha_0 = 1$. In both panels the dashed curve represents the sonic critical curve and in the bottom panel the dotted line is $v = 0$. The downstream solution is connected with various upstream solutions with light solid curves. The downstream solution is integrated numerically from $x \rightarrow 0^+$ with a LP-type solution. In both panels, the upstream solutions from top to bottom correspond to $x_{sd} = 3, 2.923, 2.773, 2.623, 2.473, 2.287, 2.2$ and 2, respectively. We note that the upstream solution with $x_{sd} = 2.287$ corresponds to a breeze. Relevant parameters are summarized in Table 1.

Table 1. Data parameters of global polytropic 'champagne flow' solutions in cases with $n = 0.9$ and $\alpha_0 = 1$.

A	B	x_{sd}	α_d	v_d	x_{su}	α_u	v_u
0.9902	−0.7699	2	0.8416	1.3019	2.0693	0.2005	−0.3012
1.3501	−0.2267	2.2	0.8172	1.4266	2.2446	0.2404	0.1004
1.5357	0	2.2869	0.8068	1.4805	2.3234	0.2586	0.2599
2.0109	0.4767	2.4732	0.7848	1.5956	2.4964	0.2993	0.5789
2.474	0.8577	2.6232	0.7678	1.688	2.6387	0.3336	0.8172
3.0224	1.2416	2.7731	0.7516	1.7803	2.7832	0.369	1.0425
3.6696	1.6323	2.9231	0.7363	1.8728	2.9292	0.4054	1.2568
4.0455	1.8367	3	0.729	1.9204	3.0047	0.4243	1.3629

by the shock conditions. This only happens when we attempt to obtain upstream variables from downstream variables. For a real x_{su}, downstream variables (x_{sd}, α_d, v_d) should satisfy

$$(1 - \gamma)\alpha_d^{\gamma-1} + 2(nx_{sd} - v_d)^2 > 0. \tag{26}$$

For $\gamma < 1$ (unphysical) and $\gamma = 1$, inequality (26) is readily satisfied; for $\gamma > 1$ or $n < 1$, this condition does not always hold. Algebraic manipulations give the downstream Mach number in the shock reference framework $\mathcal{M}_d$ as

$$\mathcal{M}_d^2 = \frac{(nx_{sd} - v_d)^2}{\gamma \alpha_d^{\gamma-1}}. \tag{27}$$

Inequality (26) imposed on a subsonic downstream Mach number is $1 > \mathcal{M}_d^2 > (\gamma - 1)/(2\gamma)$. The downstream Mach number and the upstream Mach number is related by

$$\mathcal{M}_d^2 = \frac{2 + (\gamma - 1)\mathcal{M}_u^2}{2\gamma \mathcal{M}_u^2 - (\gamma - 1)}. \tag{28}$$

This relation was provided by Lou & Cao (2008) for a relativistically hot gas and is proven valid in our model consideration. With the

possible range of upstream Mach number $1 < \mathcal{M}_u^2 < +\infty$, we then have the limit on $\mathcal{M}_d$ shown above. As we integrate LP or EdS solutions from $x = 0$ with $\alpha = \alpha_0$ and $v = 0$, solutions do not satisfy inequality (26) when x remains sufficiently small and $x_{\min 1}$ is the minimum value of x satisfying (26). This value of $x_{\min 1}$ is uniquely determined by the α_0 value. Therefore, for a fixed LP-type solution around small x, polytropic shocks can be constructed with a downstream shock in the range of $x_{\min 1} < x_{\text{sd}} < x_{\max}$, and across such a shock, the LP-type solution at small x can be matched with different asymptotic flows at large x.

Systematic numerical explorations reveal that the upstream velocity increases monotonically with the increase of x_{sd}, as shown by the variation trend of the B parameter (see Table 1). There is thus another critical value imposed on x_{sd}, denoted by $x_{\min 2}$. For $x_{\text{sd}} > x_{\min 2}$, the upstream solution matches to an asymptotic solution at large x in the form of (18) and (19) with $B > 0$, referred to as an outflow. Complementarily with $x_{\text{sd}} < x_{\min 2}$, the upstream solution matches to an asymptotic solution with $B < 0$, referred to as an inflow. As B varies continuously and monotonically with x_{sd}, for $x_{\text{sd}} = x_{\min 2}$ the upstream solution corresponds to an asymptotic solution with $B = 0$, which describes a breeze or a contraction in association with 'champagne flows'. According to asymptotic expressions (18) and (19) with $q = 0$, the breeze or contraction correspond to slow outward or inward flows. To obtain a breeze, we need a mass parameter

$$A < A_s \equiv \left[\frac{n^2}{2\gamma(3n-2)} \right]^{-1/n}. \tag{29}$$

For the specific case of $A = A_s$, either a breeze or a contraction reduces to SPS solution (17). With $n < 1$, there are three possibilities in general. First, $x_{\min 1} > x_{\min 2}$ for the allowed range to construct shocks, the upstream solutions always correspond to outflows. Secondly, $x_{\min 1} < x_{\min 2}$ for the allowed range to construct shocks, it is possible to obtain outflows, inflows and breezes or contractions for the upstream side. Thirdly, if any of $x_{\min 1}$ or $x_{\min 2}$ exceeds $x_{\max}$, a global champagne flow is not allowed. For the isothermal case of $n = 1$, we may set B equal to zero; asymptotic breezes or contractions on the upstream side are allowed, and the only allowed value of the downstream shock position is $x_{\text{sd}} = x_{\min 2}$. Shu et al. (2002) indicated that the isothermal shock position is uniquely determined by the value of α_0, which is consistent with our more general analysis here. The unique shock position found by Shu et al. (2002) corresponds to the $x_{\min 2}$ above.

The conventional scenario for 'champagne flows' would require the entire fluid to expand outward. Numerical simulations on 'champagne flows' (e.g. Tenorio-Tagle et al. 1986) assume that at $t = 0^+$ the central star is formed and the surrounding cloud is initially at rest. For $t > 0^+$, the fluid is photoionized and heated by the UV radiation from the central star and expands. In this scenario, we would require an expanding upstream flow in order to model 'champagne flows'. However, since solutions with an asymptotic inflow or contraction as upstream part may also exist, the outer part of H II regions can also have inward velocities. In fact, during the star formation even some time after the star formation, the surrounding cloud may continue to collapse towards the centre (e.g. Fatuzzo et al. 2004). With the core nuclear burning of the central protostar, the surrounding gas is ionized and heated, and the inner part of the fluid starts to expand, while the outer part continues to fall inwards. Those solutions of the LP type as the downstream side of a shock and an asymptotic inflow or contraction for the upstream side correspond

to this scenario just described; and such global solutions are referred to as inner shock expansions in a collapsing envelope (ISECE).

For the case of $n = 0.9$ and $\alpha_0 = 1$, we have determined $x_{\min 1} = 0.95$, $x_{\min 2} = 2.287$ and $x_{\max} = 3$; the shock range $2.287 < x_{\text{sd}} < 3$ gives sensible classical polytropic 'champagne flow' solutions and $0.95 < x_{\text{sd}} < 2.287$ gives the ISECE solutions as shown in Fig. 1. For $n = 0.9$, we have $A_s = 2.042$; with $x_{\text{sd}} = x_{\min 2}$ and $A = 1.536 < A_s$, the asymptotic solution is a breeze and should be considered as a classical champagne flow. Given other parameters the same, the situation of $A > A_s$ would give rise to an asymptotic contraction. The shock location and shock speed can be determined once x_{sd} is specified. The dimensionless shock position in the self-similar variable represents the shock strength and velocity in dimensional form. The shock velocity reads $\mathrm{d}r_s/\mathrm{d}t = nk_d^{1/2} x_{\text{sd}} t^{n-1}$. The outgoing shock slightly decelerates (for n slightly less than 1) and the shock velocity is proportional to x_{sd}.

As shown in Fig. 1 and Table 1, with increasing x_{sd}, the upstream variables at the shock front v_u and α_u increase, and the two parameters A and B of asymptotic solutions (18) and (19) also increase. This is a fairly common feature, observed in all other cases that we have studied numerically. Different shock positions match with different asymptotic solutions at large x. Once A and B are specified, the shock position x_{sd} is uniquely determined. As A is the mass parameter and B is the velocity parameter, x_{sd}, proportional to the shock velocity and strength, is determined not only by initial mass density but also by the initial motion. This differs from the isothermal case when $B = 0$ with the mass parameter A determining the shock behaviour. We expect a faster and stronger shock with a higher initial speed.

We further identify two subtypes of such ISECE solutions: (i) the upstream side has an outward velocity near the shock and an asymptotic inward velocity far from the centre (e.g. solution with $x_{\text{sd}} = 2.2$ in Fig. 1); (ii) the upstream side has an inward velocity everywhere (e.g. solution with $x_{\text{sd}} = 2$ in Fig. 1). For the type (i) solutions, there is a stagnation point x_{stg} where the radial flow velocity vanishes; for the solution with $x_{\text{sd}} = 2.2$, $x_{\text{stg}} \sim 3$. With self-similar transformation (7), this stagnation point $r_{\text{stg}} = k^{1/2} t^n x_{\text{stg}}$ travels outward with time in a self-similar manner.

For ISECE solutions, we envision that such solutions correspond to the situation where a star starts to burn, ionizing and heating the surrounding medium as the gas falling continues. The gas infall and collapse are indispensable in star formation. If the nascent star ionizes the whole residual gas sufficiently fast, the outer gas may still possess an inward momentum. A champagne shock runs into the infall gas, deposits outward momentum and accelerates the outer gas. If a shock is sufficiently strong, we expect type (i) solutions, e.g. the gas immediately outside a shock flows outward, and the stagnation point travels outward proportional to the self-similar expansion of the shock. If a shock is sufficiently weak, we expect type (ii) solutions, e.g. the gas flows inward outside the shock front. This ISECE scenario is expected to occur in certain H II regions (e.g. Fatuzzo, Adams & Myers 2004; Shen & Lou 2004).

3.2 Cases of a fixed dimensionless shock position

The variation of LP-type solutions with different α_0 and the same x_{sd} is shown in Fig. 2. For $\alpha_0 > 2/3$, α decreases with increasing x while for $\alpha_0 < 2/3$, α increases with increasing x. With a larger α_0 the LP-type solution encounters the sonic critical curve earlier; therefore α_0 cannot be too large, otherwise the LP-type solution encounters the sonic critical curve before reaching the pre-set shock position x_{sd}.
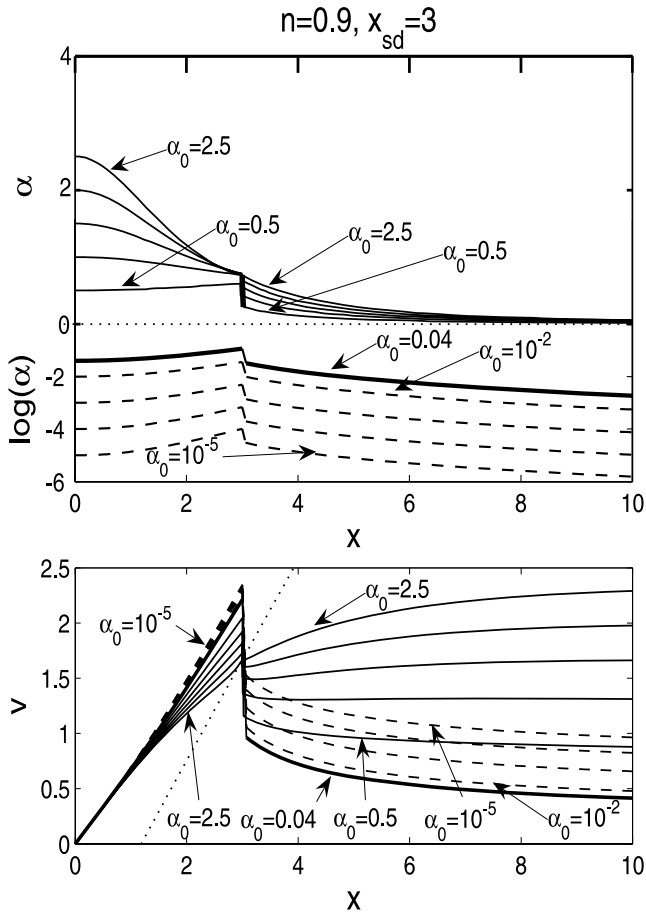
Figure 2. The reduced mass density $\alpha(x)$ (top) and the reduced radial flow velocity $v(x)$ (bottom) for global polytropic 'champagne flow' solutions in cases $n = 0.9$ (thus $\gamma = 1.1$) and $x_{sd} = 3$. In the top panel, the horizontal dotted line stands for $\alpha = 0$, separating the top panel into two parts; the vertical scales in these parts are different. In the upper part $\alpha(x)$ is presented linearly, while in the lower part $\log[\alpha(x)]$ is presented. In the bottom panel, the dotted line is the sonic critical curve. Shocks at $x \sim 3$ as the discontinuity in solutions are shown. The solid curves on the downstream side of shocks are LP-type solutions with $\alpha_0 = 0.5, 1, 1.5, 2$ and 2.5 (from bottom to top in the top panel and from top to bottom in the bottom panel). The solid curves on the right show, respectively, the corresponding upstream solutions approaching different asymptotic solutions at large x (from bottom to top in the top panel and from bottom to top in the bottom panel). The dashed curves on the downstream side of shocks are LP-type solutions with $\alpha_0 = 10^{-5}, 10^{-4}, 10^{-3}$ and 10^{-2} (from bottom to top in the top panel and from top to bottom in the bottom panel). The dashed curves on the right show, respectively, the corresponding upstream solutions approaching different asymptotic solutions at large x (from bottom to top in the top panel and from top to bottom in the bottom panel). The thick solid curve in both panels represents the solution with $\alpha_0 = 0.04$, which has the lowest upstream speed and the minimum B at large x. Relevant parameters are summarized in Table 2.

One case of $n = 0.9$ and $x_{sd} = 3$ is shown in Fig. 2 with parameters given in Table 2. Here, we have $\alpha_{sd} < 2.5$.

As shown in Fig. 2 and Table 2, with the increase of α_0, the upstream conditions at the shock front α_u and the mass parameter A of the asymptotic solution increases, but v_u and B do not have a steady trend. As α_0 increases from 10^{-5} to 0.04, v_u and B decrease, while as α_0 increases from 0.04 to 2.5, v_u and B increase (see Table 2). This shows that v_u and B are correlated. The minimum

values of v_u and B are associated with $\alpha_0 = 0.04$. Here we show that with a prefixed downstream shock position x_{sd}, it is possible that neither breeze nor contraction solutions are allowed. With a x_{sd} as large as 3, all the asymptotic upstream solutions correspond to outflows. In the isothermal analysis of Shu et al. (2002), the mass parameter A tends to zero with $\alpha_0 \rightarrow 0^+$. In polytropic cases, we obtain similar results. According to series expansions (24) and (25), if setting $\alpha_0 = 0$ exactly, the integration gives a trivial solution of $\alpha = 0$.

Based on numerical explorations for $\alpha_0 \rightarrow 0^+$ in isothermal cases, Shu et al. (2002) argued that the self-gravity may be neglected for cases with small central density, and developed another self-similar transformation, viz., the so-called invariant form, in order to model the initial mass density profile other than that of a SIS (i.e. $\rho \propto r^{-2}$). The initial mass density profile $\rho \propto r^{-l}$, where index l does not necessarily equal to 2, can be described by the invariant form when the self-gravity is ignored. We perform a similar reduction with the invariant self-similar transformation for a conventional polytropic gas without the self-gravity (see Appendix A), and show that with $n \neq 1$ (i.e. non-isothermal cases), the power index l must be equal to $2/n$ for a self-similar form. This mass density profile with a scaling index $l = 2/n$ is the same as that in a SPS and in asymptotic solutions at large x. In summary, the freedom of choosing l in the invariant form disappears for non-isothermal cases. From another perspective, since the index n ranges in $2/3 < n < 4/3$, self-similar polytropic champagne flows can model the initial mass density profile with $3/2 < l < 3$. In other words, the objective to model the initial density profile other than $l = 2$ is naturally fulfilled, without the necessity of dropping the self-gravity. The clear advantage of our polytropic approach is that the self-gravity is included in the model consideration. Therefore, to apply our polytropic solutions, $\alpha_0 \rightarrow 0^+$ is no longer required. From transformation (7), parameter α_0 is tightly linked with the central mass density ρ_0 and time-scale t, and should have different values in different situations. Therefore, polytropic champagne flow solutions are adaptable to a much wider range of astrophysical cloud systems. Moreover, the $\alpha_0 \rightarrow 0^+$ cases in our polytropic framework can be approximated by a central 'void' as discussed in the following section. With a central 'void', we are able to neglect the gravity of the central region where the density is sufficiently low and still consider the self-gravity of the outer more dense gas medium.

In the isothermal case of Shu et al. (2002), the solution in which the outer part is a static SIS represents a limiting solution defining the maximum value of α_0. In the polytropic cases with $n = 0.9$, we can also identify such a limit by requiring $B = 0$ for the upstream asymptotic solutions, such that for a pre-set α_0 the downstream shock position x_{sd} is uniquely determined. A family of such 'champagne flow' solutions with asymptotic upstream breezes or contractions is shown by solid curves in Fig. 3 with parameters summarized in Table 3. With a gradual increase of α_0, the upstream side varies from outward breezes, to a SPS, and to an inward contraction; this trend leads to a maximum α_0 if we define an outward breeze for classical 'champagne flows'. Here, the critical value $\alpha_0 = 3.13$ for an upstream SPS corresponds to the upstream SIS limit in Shu et al. (2002) (i.e. $\alpha_0 = 7.9$ in the isothermal case). Naturally, this critical value depends on the choice of n. For $\alpha_0 > 3.13$, an upstream asymptotic contraction or an ISECE solution appears (dashed curve in Fig. 3). Thus, isothermal champagne flows form a special family with $B = 0$ and $n = 1$, referred to as breeze champagne flows. With $2/3 < n < 1$ or $2 < l < 3$, there are many more physically possible champagne flows, for which the upstream side corresponds to asymptotic outflows at large x. The physical meaning of this special

Table 2. Data parameters of global polytropic 'champagne flow' solutions in cases with $n = 0.9$ and $x_{sd} = 3$.

α_0	A	B	x_{sd}	α_d	v_d	x_{su}	α_u	v_u
0.00001	0.0002532	1.145	3	0.0001	2.3469	3.0609	0.000030184	1.5294
0.0001	0.001735	0.9499	3	0.0007	2.3152	3.064	0.0001993	1.3959
0.001	0.01243	0.7205	3	0.0049	2.2821	3.0693	0.001372	1.2353
0.01	0.0912	0.4713	3	0.0358	2.2449	3.0746	0.009752	1.0536
0.04	0.3045	0.3899	3	0.1154	2.2135	3.0715	0.03192	0.9641
0.5	2.4053	1.1453	3	0.6048	2.0444	3.0197	0.2556	1.1567
1	4.0455	1.8367	3	0.729	1.9204	3.0047	0.4244	1.3629
1.5	5.5009	2.406	3	0.7512	1.8166	3.008	0.5556	1.5059
2	6.9587	2.9308	3	0.7414	1.7274	3	0.6606	1.6083
2.5	8.5684	3.4633	3	0.7588	1.562	2.8444	0.7086	1.4913
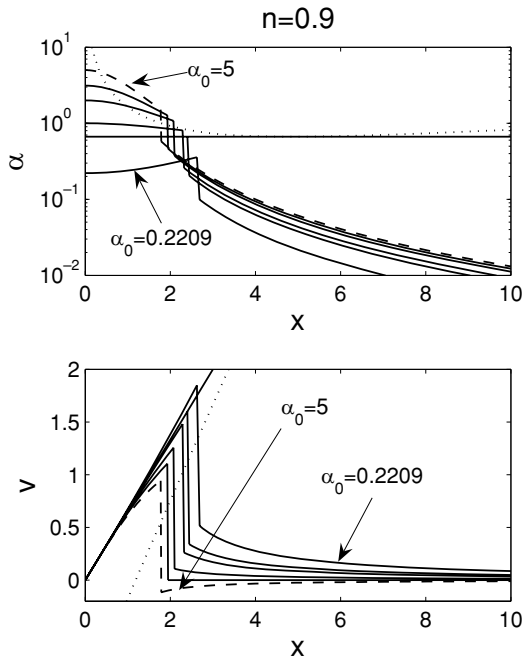
Figure 3. 'Champagne flow' solution with a LP-type downstream and the upstream part as a breeze or contraction for $n = 0.9$ (thus $\gamma = 1.1$). The top panel shows the density and the bottom panel shows the velocity. In both panels the dotted curve is the sonic critical curve. The solutions are integrated from $\alpha_0 = 0.2209, 2/3, 1, 2, 3.13$ and 5 (from bottom to top in the top panel and from top to bottom in the bottom panel), and the downstream shock positions x_{sd} are carefully chosen to let the upstream solution correspond to the asymptotic solutions with $B = 0$. Relevant parameters are summarized in Table 3. For the solution with $\alpha_0 = 3.13$, the corresponding upstream is a SPS. For $\alpha_0 > 3.13$, the upstream contracts (dashed curve), while for $\alpha_0 < 3.13$, the upstream is a breeze.

solution whose upstream side is the outer part of a static SPS is clear: the outer envelope of gas is initially in a hydrostatic equilibrium, and the expanding shock created by the UV photoionization travels into the static envelope; on the downstream side of this expanding shock, the gas is heated to high temperatures. As the static SPS relies on the scaling parameter n or the polytropic index γ, we expect one single solution for a pre-set n. From Table 3 we see clearly that with the increase of α_0, the downstream shock position to obtain a breeze in the upstream, or x_{min2} decreases. Meanwhile, numerical explorations suggest that x_{min1} increases with increasing

Table 3. Parameters of global polytropic 'champagne flow' solutions with $n = 0.9$ and upstream breeze or contraction ($B = 0$).

α_0	A	B	x_{sd}	α_d	v_d	x_{su}	α_u	v_u
0.2209	0.7550	0	2.6250	0.3571	1.8473	2.6873	0.0990	0.5153
2/3	1.3240	0	2.3986	0.6667	1.5991	2.4419	0.2045	0.3407
1	1.5357	0	2.2869	0.8068	1.4805	2.3234	0.2586	0.2599
2	1.8643	0	2.0733	1.0783	1.2563	2.0996	0.3734	0.1069
3.13	2.0420	0	1.9264	1.2773	1.1036	1.9475	0.4643	0
5	2.1924	0	1.7706	1.5091	0.9429	1.7873	0.5746	−0.1163

α_0. Hence we expect for a sufficiently large α_0, x_{min2} would become less than x_{min1} to forbid ISECE solutions.

4 SIMILARITY POLYTROPIC 'CHAMPAGNE FLOWS' WITH CENTRAL VOIDS

We now establish and analyse a new class of 'champagne flow' solutions with voids surrounding the centre. We extend solutions from $x = 0$ to the dimensionless self-similar expanding boundary x^* of a void, inside of which there is no mass, i.e. $m^* = m(x^*) = 0$. In our notations, superscript* attached to variables indicates variables on the void boundary x^*. By expression (8), we have $v^* = nx^*$. The void boundary conditions are

$$\alpha = \alpha^*, \qquad v = nx^* \qquad \text{at} \qquad x = x^*. \tag{30}$$

A Taylor series expansion to the first order around the void boundary $x = x^*$ of ODEs (12) and (13) yields

$$v(x) = nx^* + 2(1 - n)(x - x^*) + \cdots, \tag{31}$$

$$\alpha(x) = \alpha^* + \frac{n(1 - n)}{\gamma}(\alpha^*)^n x^*(x - x^*) + \cdots. \tag{32}$$

Series expansions (31) and (32) are conspicuously different from series expansions (24) and (25). The proportional coefficient of the asymptotic velocity is no longer 2/3 but depends on the scaling index n. By translating the origin, the dynamic flow behaves differently. For $n < 2$, solutions given by expression (31) are locally above the line $nx - v = 0$, indicating a positive enclosed mass. Numerical integrations reveal that the solutions are always above the line $nx - v = 0$ thereafter. Here, we model a gas flow with a central void in the presence of self-gravity and thermal pressure, directly relevant to galactic subsystems such as H II regions.

One can readily obtain the downstream portion of 'champagne flow' solutions by numerically integrating coupled non-linear ODEs
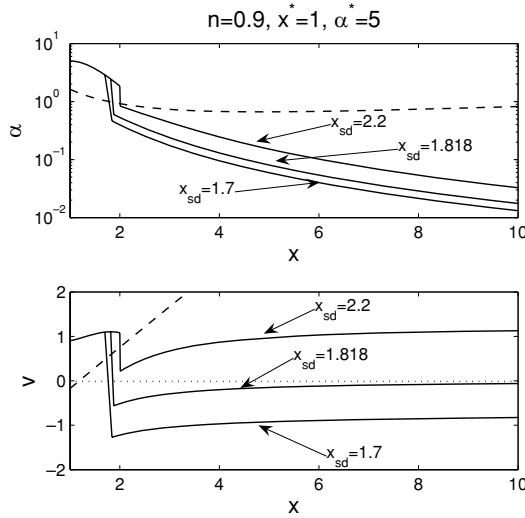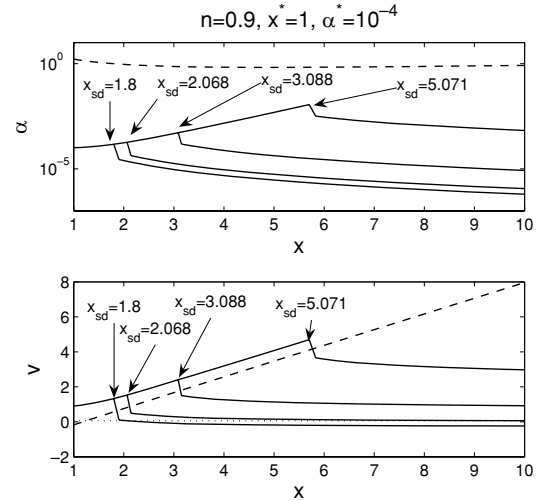
Figure 4. The reduced mass density $\alpha(x)$ (top) and the reduced radial flow velocity $v(x)$ (bottom) for semicomplete 'champagne flow' solutions with a central void inside $x^* = 1$ in the case of $n = 0.9$ and density on the void boundary $\alpha^* = 5$. In both panels, the dashed curve stands for the sonic critical curve. In the bottom panel the dotted line stands for the line $v = 0$. The solid curve on the upper left of the sonic critical curve is the downstream void solution and the solid curves on the lower right of the sonic critical curve are the corresponding upstream solutions with the downstream shock position $x_{sd} = 1.7$ (inflow), 1.818 (contraction) and 2 (outflow). In this case, $x_{min2} \approx 1.818$ and $x_{min1} = 1.408$. Numerical data about these solutions are tabulated in Table 4.

Figure 5. The reduced mass density $\alpha(x)$ (top) and the reduced radial velocity $v(x)$ (bottom) for semicomplete 'champagne flow' solutions with a central void inside $x^* = 1$ in cases with $n = 0.9$ (thus $\gamma = 1.1$) and a density on the void boundary $\alpha^* = 10^{-4}$. In both panels, the dashed curve represents the sonic critical curve. In the bottom panel, the dotted line stands for the line $v = 0$. The solid curve on the left-hand side is the downstream void solution and the solid curves on the right-hand side are the corresponding upstream outflow solutions with the downstream shock position $x_{sd} = 1.8$ (inflow), 2.068 (breeze), 3.088 (outflow) and 5.701 (outflow). Here, $x_{sd} = 2.068$ is the limit to ensure an asymptotic outflow, i.e. $x_{min2} \approx 2.068$. In this case, $x_{min1} = 1.261$. Numerical data for these solutions are tabulated in Table 4.

(12) and (13) from the void boundary x^* with asymptotic expansions (31) and (32). All such void solutions encounter the sonic critical curve, and the lower the value of α^* is, the later (or at larger x) the void solution encounters the sonic critical curve. In order to match with asymptotic solutions of finite density and velocity at large x, void solutions must either cross the critical curve smoothly or connect to another branch of solutions via shocks. To model 'champagne flows', we need to construct shocks to obtain global solutions. Global void solutions that cross the sonic critical curve smoothly will be discussed in Lou & Hu (2008). We now present the solutions for large and small α^*, respectively. A family of semicomplete 'champagne flow' solutions with $n = 0.9$, void boundary $x^* = 1$ and $\alpha^* = 5$ is constructed by varying the self-similar shock position as shown in Fig. 4. Complementarily, another family of solutions with $\alpha^* = 10^{-4}$ is also constructed and shown in Fig. 5. Both outflow, inflow and breeze or contraction as the upstream side are presented. Relevant parameters of these void 'champagne flow' solutions are summarized in Table 4.

Similar to no void cases, α decreases with increasing x for large α^*, so the density on the void boundary is a local maximum (see

Fig. 4); while for small α^*, α increases with increasing x, so the density maximum is at the downstream side of the shock. The latter corresponds to a shell-like structure in self-similar expansion (see Fig. 5).

With downstream void solutions and upstream outflow and breeze solutions connected by shocks, we establish semicomplete polytropic 'champagne flow' solutions with central voids. Similar to LP-type solutions with shocks, there are also one maximum x_{max} and two minimum limits x_{min1} and x_{min2} imposed on the downstream shock position x_{sd} in order to obtain 'champagne flow' solutions. Systematic numerical explorations for cases of $n = 0.7, 0.8$ and 0.9 show that in general $x_{min2} > x_{min1}$. For $x_{min1} < x_{sd} < x_{min2}$, a void solution can be matched with an asymptotic inflow to produce ISECE solutions, while for $x_{sd} > x_{min2}$, a central void solution can be matched with an asymptotic outflow to produce 'champagne flow' solutions. For $x_{sd} = x_{min2}$, the upstream corresponds to a breeze or a contraction with $B = 0$. The analysis here parallels that in the previous section for cases without central voids; in particular, the parameters x_{min1} and x_{min2} are determined not only by n and α^*, but also by the expanding void boundary x^*. Numerical explorations

Table 4. Polytropic 'champagne flow' solutions with a central void inside $x^* = 1$ in the case of $n = 0.9$.

α^*	A	B	x_{sd}	α_d	v_d	x_{su}	α_u	v_u
10^{-4}	0.000 106	-0.3813	1.8	$1.4\,734 \times 10^{-4}$	1.3322	1.9058	$2.7\,895 \times 10^{-5}$	0.1058
10^{-4}	0.000 191	0	2.068	$1.8\,377 \times 10^{-4}$	1.5386	2.1442	$4.2\,673 \times 10^{-5}$	0.4893
10^{-4}	0.0014	1.0833	3.088	0.000 517	2.398	3.152	0.00015	1.501
10^{-4}	0.0991	3.5315	5.701	0.0114	4.701	5.839	0.0032	3.669
5	2.2512	-1.0512	1.7	2.8906	1.0956	1.8424	0.4646	-1.2708
5	2.9388	0	1.818	2.4535	1.1047	1.8777	0.5978	-0.5632
5	5.2894	1.7273	2	1.8447	1.0816	2.0101	0.8364	0.2166

suggest that for a certain n, with the increase of α^*, $x_{\min 1}$ increases and $x_{\min 2}$ decreases. Hence for a sufficiently large α^*, we expect $x_{\min 2} < x_{\min 1}$ for which ISECE solutions are not allowed. This is consistent with polytropic cases without central voids.

5 ANALYSIS AND DISCUSSION

5.1 Comparison with numerical simulations

To adapt our self-similar solutions for modelling an astrophysical cloud system, we need to first specify the parameter k related to the sound speed squared. By varying k, one can model clouds of different scales using a single self-similar solution. Parameter k is determined by the thermodynamic parameters, including thermal pressure p, mass density ρ and temperature T. A useful relation for a conventional polytropic gas derived from transformation (7) is

$$k = \frac{p}{\rho^\gamma (4\pi G)^{\gamma-1}} = \frac{k_B T}{\mu \rho^{\gamma-1}(4\pi G)^{\gamma-1}}, \tag{33}$$

where μ is the mean molecular mass of gas particles. For a typical value provided by the classification of Habing & Israel (1979), the UC H II regions have an electron number density $n_e > 3000 \text{ cm}^{-3}$ (corresponding to a mass density $\rho > 5 \times 10^{-21} \text{ g cm}^{-3}$ for a fully ionized hydrogen gas) and the compact H II regions have $1000 < n_e < 3000 \text{ cm}^{-3}$ (corresponding to $1.7 \times 10^{-21} < \rho < 5 \times 10^{-21} \text{ g cm}^{-3}$ for mass density ρ). Typically, the temperature of H II regions is of order of $\sim 10^4$ K. For a fully ionized hydrogen gas, we assume that $\mu = m_p/2$, where m_p is the proton mass. The value of the polytropic index γ does influence very much the resulting k and thus k should be evaluated specifically. For nearly isothermal cases, with relation (33), we estimate k for UC and compact H II regions to be $k \sim 10^{11} \sim 10^{12}$ cgs unit. One should be aware that κ and thus k vary with the gas temperature and density in a cloud. Here, we presume a constant k to convert self-similar variables to real space variables as a first approximation.

We now compare our self-similar solutions of quasi-spherical symmetry with previous numerical simulations. Tenorio-Tagle et al. (1986) performed a numerical study for a similar scenario as ours, i.e. a nascent central massive protostar ionizes and heats the ambient neutral gas and then leads to 'champagne flows'. In their simulation, the radiative cooling rate is assumed to be low and thus our polytropic approach may be applicable. Franco et al. (1990) gave an analytical model for the formation and expansion of H II regions and have their solutions compared with simulations. We intend to demonstrate that our self-similar polytropic analysis of the problem gives qualitatively similar results.

In the simulation of Tenorio-Tagle et al. (1986), computations were carried out following the progressive ionization of a diffuse gas and subsequent dynamical evolution, in a globular cluster soon after the star formation has been initiated. The residual gas is initially in a hydrostatic equilibrium in the gravitational field at a uniform temperature and all the ionizing UV radiation comes from stars at the very centre of the cluster. We emphasize that only the cases in which the gas is fully ionized correspond to our conventional 'polytropic champagne flow' model. In the simulation, the initial mass density at the centre ρ_0, initial temperature T_0 and the UV photon flux F from the central star completely determine the evolution in spherical symmetry. To translate these parameters into our self-similar form of solutions, we first explore the time evolution of a 'champagne flow' shock. In our self-similar model, the shock radius r_s obeys $r_s = k^{1/2} x_s t^n$. With such a self-similar formula, we can fit the scaling index n and $k^{1/2} x_s$ to shock positions obtained by the numerical
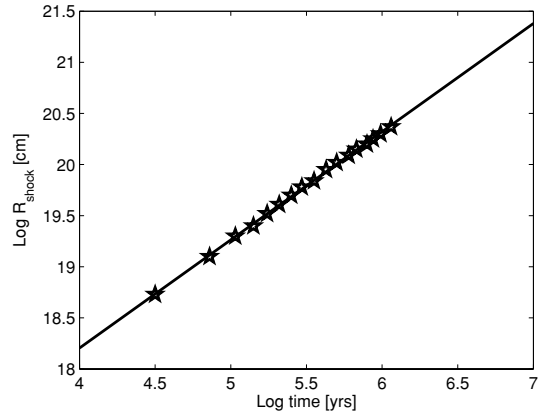

Figure 6. Shock position evolution with time t in a 'champagne flow' for our self-similar model (solid line) and the numerical simulation of Tenorio-Tagle et al. (1986) (asterisks). For the simulation, the adopted parameters are central initial density $\rho_0 = 2 \times 10^{-21} \text{ g cm}^{-3}$, initial temperature $T_0 = 3000$ K and the ionization UV flux $F = 2 \times 10^{51}$ photon s^{-1}. For the self-similar model, the best-fitting parameters are $n = 1.0583$ and $\log(k^{1/2} x_s) = 6.0356$ in cgs unit.

simulation for case F of Tenorio-Tagle et al. (1986), and the result comparison is shown in Fig. 6 with relevant parameters in caption. We see an almost perfect fit, suggesting that the dynamical evolution of 'champagne flows' approaches a self-similar form. This fitting gives a value of $n = 1.0583$ and $\log(k^{1/2} x_s) = 6.0356$ in cgs unit (strictly speaking, we need a general polytropic gas for $\gamma > 1$). The value of n is fairly close to the isothermal case of $n = 1$, consistent with the model analysis of the numerical simulation that the gas evolution is nearly isothermal (Tenorio-Tagle et al. 1986).

We now generate a global 'champagne flow' solution grossly comparable to fig. 2 of Tenorio-Tagle et al. (1986) by fitting parameters. We first choose a central reduced density $\alpha_0 \sim 1 \times 10^{-5}$ such that the initial central density yields the value used in the simulation. We expediently choose $n = 0.9$ (hence the parameter $\gamma = 2 - n = 1.1$) to model the initial density profile $l = -2/n = -2.22$. Note that parameter n for the 'champagne flow' solution is slightly different from the value we obtain from the fitting. With ρ_0 and T_0 specified in the simulation, we estimate $k_d = 3.6 \times 10^{15}$ cgs unit with expression (33). We still have the freedom to require the shock travelling to $r_s = 2.51 \times 10^{19}$ cm at $t = 1.3 \times 10^5$ yr, giving $x_{sd} = 1.86$. With these parameters, we model 'champagne flows' in diffuse H II regions with radius r up to 10^{21} cm (i.e. ~ 300 pc). The full solution is shown in Fig. 7. The time-scale of 1.3×10^5 yr is regarded as the duration of the formation phase and the initial time for a 'champagne flow', and the time-scale 5.1×10^6 yr is regarded as the lifetime of a 'champagne flow'.

The orders of magnitude of all variables are consistent with typical values; e.g. the expansion velocity is several tens km s^{-1} and the temperature is about $\sim 10^4$ K. The enclosed mass at $r = 10^{21}$ cm (~ 300 pc) is about $850 \text{ M}_\odot$, consistent with the value of $\sim 800 \text{ M}_\odot$ given by the numerical simulation and with the typical value for diffuse H II regions. The enclosed mass does not vary with time t, confirming the cut-off radius chosen at $r = 10^{21}$ cm. As time evolves, the central number density decreases from $10^{-0.5}$ to $10^{-3.5} \text{ cm}^{-3}$ and the central thermal pressure decreases accordingly from 10^{-12} to 10^{-15} dyne cm^{-2}.

We can also compare variable profiles with the case F of Tenorio-Tagle et al. (1986). The velocity profiles are very similar and we clearly see an expanding shock. As time evolves, the shock strength
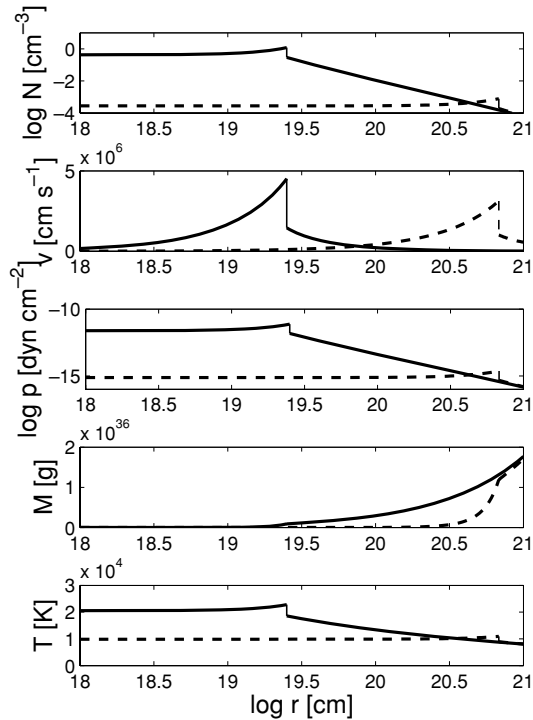
Figure 7. Self-similar 'champagne flow' solutions for radius up to 10^{21} cm ($\sim$300 pc) at time $t = 1.3 \times 10^5$ yr (solid curves) and $t = 5.1 \times 10^6$ yr (dashed curves). From top to bottom, the panels show number density, velocity, pressure, enclosed mass and temperature of the gas, respectively. The self-similar shock solution is obtained with $n = 0.9, \gamma = 1.1, \alpha_0 = 1 \times 10^{-5}$ and downstream shock position $x_{sd} = 1.86$. The downstream sound scaling factor k_d is 3.6×10^{15} cgs unit, and the upstream sound scaling factor k_u is 3.38×10^{15} cgs unit. The self-similar variables on the downstream side of the shock are $(x_{sd}, \alpha_d, v_d) = (1.86, 2.80 \times 10^{-5}, 1.37)$, and the corresponding upstream variables are $(x_{su}, \alpha_u, v_u) = (1.92, 6.88 \times 10^{-6}, 0.46)$. At large x, the numerical solution matches with asymptotic solution (18) and (19) with $A = 31.942$ and $B = 1.006$ at large x.

becomes weaker. In both numerical simulation and our model analysis, we observe a density peak on the downstream side of the shock and a significant temperature gradient on the upstream side, which cannot be accounted for by previous isothermal solutions. The upstream density and pressure profiles are also similar; however, the downstream density, pressure and temperature profiles (near centre) are somewhat different. In Tenorio-Tagle et al. (1986), temperature, pressure and density are initially very uniform behind the champagne shock but at the end of the calculations show large inward gradients. In Fig. 7, our model also produces quasi-uniform temperature, pressure and density behind the shock at the beginning ($t = 1.3 \times 10^5$ yr), but we do not observe large inward gradients at the end. These differences are primarily due to the different physical assumptions adopted in the simulation and our self-similar solutions. Tenorio-Tagle et al. (1986) treated the gas dynamics in protoglobular clusters and neglected the gas self-gravity as the gas mass is only about 0.1 per cent that of the stars. As shown above, our self-similar solutions neglect the gravity of the central massive protostar but include the self-gravity effect. Another important factor that introduces such difference is that in the simulation both forward champagne shock and reverse rarefaction wave are taken into account. Our self-similar model can accommodate forward moving shock, so we only have the principle outgoing champagne shock.

We calculate the total energy E_{total} defined as the energy of the gas under consideration in an infinite space. The total energy at time t can be expressed as

$$E_{total} = E_K + E_G + E_I$$

$$= \int_{r_{in}}^{r_{out}} \left(\frac{1}{2}\rho u^2 - \frac{GM\rho}{r} + \frac{i}{2}p \right) 4\pi r^2 \, dr$$

$$= \frac{k^{5/2} t^{5n-4}}{2G} \int_{x_{in}}^{x_{out}} \left[\alpha v^2 x^2 - \frac{2}{(3n-2)} \alpha^2 x^3 (nx - v) \right.$$

$$\left. + i\alpha^\gamma x^2 \right] dx, \tag{34}$$

where E_K, E_G and E_I are the kinetic, gravitational and internal energies of the gas, respectively, $r_{in}, r_{out}, x_{in}, x_{out}$ are the inner and outer boundaries of the gas under consideration and i is the degree of freedom of the gas particle presumed to be 3. Note that one fixed r_{out} at different times corresponds to different values of x_{out}. In this solution, $E_{total} = 5.5 \times 10^{48}$ erg at $t = 1.3 \times 10^5$ yr, and $E_{total} = 8.1 \times 10^{48}$ erg at $t = 5.1 \times 10^6$ yr, so there is net energy input. Especially, we see the kinetic energy $E_K = 6.4 \times 10^{47}$ erg at $t = 1.3 \times 10^5$ yr, indicating a small fraction of the total energy, and $E_K = 3.9 \times 10^{48}$ erg at $t = 5.1 \times 10^6$ yr, indicating a fairly large fraction of the total energy. The increase of kinetic energy shows clearly the development of a champagne flow. The gravitational energy is of order 10^{44} erg, much less than the kinetic energy throughout this duration. This confirms that the gas is not bounded and must have an outflow. We are also able to consider qualitatively the local energy exchange throughout the self-gravitating gas with relation (16). In Fig. 7, $\partial p/\partial r$ is positive on the downstream side and negative on the upstream side. For $\gamma = 1.1$, the downstream and upstream sides locally loses and gains energy, respectively. In summary, the profiles on the order of magnitudes, and the time evolution of our self-similar solution in modelling this case are grossly consistent with the numerical simulation result of Tenorio-Tagle et al. (1986), which lends support to our polytropic self-similar 'champagne flow' solution as a gross description of dynamics of H II regions.

Recent studies further suggest that the inclusion of stellar winds is also important and even necessary sometimes in understanding the large-scale dynamics of H II regions. Comerón (1997) found that a shocked stellar wind in the central region produces important morphological differences as compared to windless cases. Moreover, Comerón (1997) suggested that the spatial scale of an H II region undergoing 'champagne flow' is systematically larger and the gas flow is generally faster as driven by a central stellar wind. Arthur & Hoare (2006) provided two-dimensional cylindrical radiative–hydrodynamic simulations of cometary H II regions using champagne flow models, by taking into account of strong stellar winds from the central ionizing star. In these simulations, the hydrodynamics and radiative transfer are coupled through an energy equation whose source term depends on the photoionization heating and radiative cooling rates; while with our polytropic approach, complicated energetic processes are relegated to the choice of γ. Arthur & Hoare (2006) studied the hydrodynamics of a compact H II region with a radius 0.13 pc and at a time $\sim$200 yr after the triggering of UV ionizing photons and powerful stellar winds; a stellar wind bubble around the centre with a radius up to 0.03 pc is formed. Inside such a stellar wind bubble, the mass density is about three orders of magnitude lower than that of the surrounding medium, and the density of the flow does not vary much with radius in the vicinity of the bubble boundary. Because the central wind bubble is effectively depleted of mass and the gravity force of the central
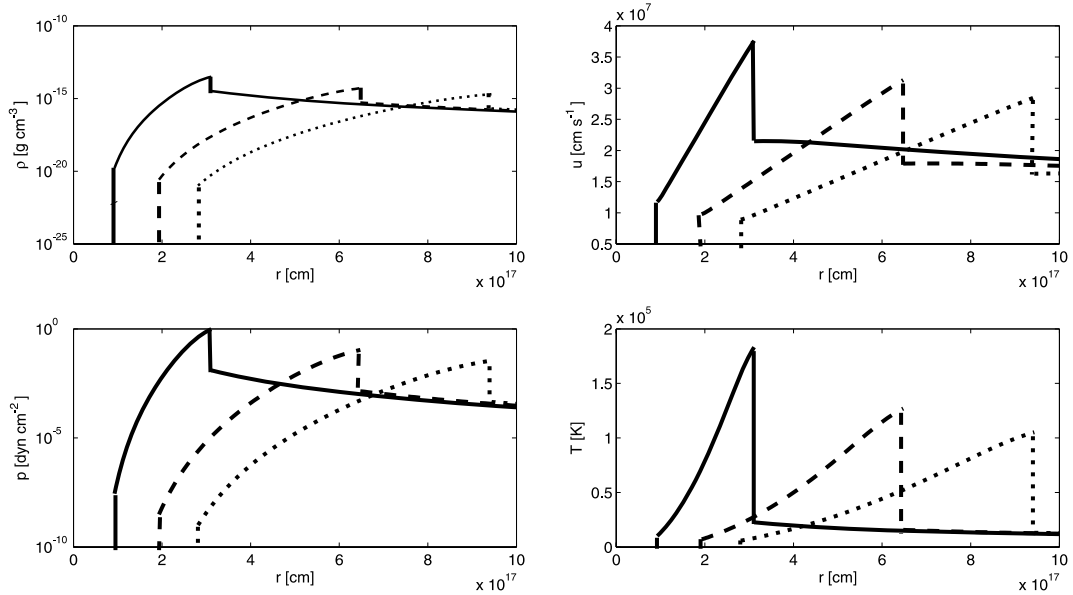
Figure 8. Self-similar 'champagne flow' solution with an initial central void radius of 10^{17} cm at time 200 yr (solid curve), 500 yr (dashed curve) and 800 yr (dotted curve). The four panels show mass density ρ, flow velocity u, thermal pressure p and temperature T of the gas, respectively. The central void has a radius of $x^* = 2.68$, corresponding to $r^* = 0.03, 0.06, 0.09$ pc with increasing time t. The self-similar solution is obtained with parameters: $n = 0.8$, $\gamma = 1.2$, $\alpha^* = 5.5 \times 10^{-7}$ and downstream shock position $x_{sd} = 9$. The downstream sound parameter k_d is 2.5×10^{17} cgs unit, and the upstream sound parameter k_u is 4.9×10^{16} cgs unit. The self-similar variables on the downstream side of the shock are $(x_{sd}, \alpha_d, v_d) = (9, 1.07, 6.86)$, and the corresponding upstream variables are $(x_{su}, \alpha_u, v_u) = (20.4, 0.111, 8.88)$. At large x, the solution matches with asymptotic solution (18) and (19) with $A = 135$ and $B = 22$ at large x. The enclosed mass by radius of 10^{18} cm is 1.38×10^6, 1.23×10^6 and 1.06×10^6 $M_\odot$ as time evolves. The total energy of gas is 5.86×10^{53}, 5.94×10^{53} and 5.98×10^{53} erg, respectively.

massive star may be neglected, given a typical Bondi–Parker radius of $\sim 10^2$ au, we thus approximate such a stellar wind bubble as a central 'void' and model it using our polytropic self-similar void 'champagne flow' model.

In the scenario as outlined by Arthur & Hoare (2006), the central star has an effective temperature $T_{\text{eff}} = 3 \times 10^4$ K, a stellar wind mass-loss rate $\dot{M} = 10^{-6}$ $M_\odot$ yr^{-1} and a terminal wind speed $V_w = 2000$ km s^{-1}. The initial ambient medium has a number density of $n_0 = 6000$ cm^{-3} and a temperature of $T_0 = 300$ K. In our self-similar model for 'champagne flows', the radius of a void boundary is $r^* = k^{1/2} x^* t^n$. By taking $n = 0.8$, we have $k^{1/2} x^* = 1.34 \times 10^9$ cgs unit to obtain a $r^* = 0.03$ pc central void at a time of $t = 200$ yr. The n value depends on the energetic process, including plasma cooling and radiative heating, of the flow. We further estimate from relation (33) for a downstream sound parameter $k_d = 2.5 \times 10^{17}$ cgs unit, and for a self-similar void boundary $x^* = 2.68$. Another parameter that needs to be specified is the mass density on the expanding void boundary, denoted as α^* here. The simulation of Arthur & Hoare (2006) gives an electron number density on the void boundary as $n_e^* = 10^4$ cm^{-3} at $t = 200$ yr. With relation $\rho^* = \alpha^*/(4\pi G t^2)$, we estimate $\alpha^* = 5.5 \times 10^{-7}$. We emphasize that the length and time-scales in this case are quite different from those in the previous case of Tenorio-Tagle et al. (1986). As an important advantage, this suggests that self-similar models are suitable to give a unified description for cloud systems on quite different scales.

As $n < 1$ in this case, we have one more degree of freedom to specify the shock position. In principle, the shock position is determined by both the initial density (mass parameter A) and the initial gas motion (velocity parameter B). We find that the lower limit of the downstream shock position x_{sd} is 8.8, according to condition (26); thus, the minimum shock position at $t = 200$ yr is $\sim 3.04 \times 10^{17}$ cm (i.e. about 0.1 pc). The numerical simulation of Arthur &

Hoare (2006) studied the gas dynamics up to a radius of 0.13 pc. As an example of illustration, we assume $x_{sd} = 9$ and show the resulting solution in Fig. 8. This solution clearly shows that as time evolves, the void boundary expands, meanwhile the density and pressure in the vicinity of void boundary decrease by several orders of magnitude, consistent with the simulation. However, we see a very high density near the 'champagne flow' shock on the downstream side, and as time evolves, the density profile becomes more and more smooth. For our self-similar 'champagne flow' model with central expanding voids, the velocity can rise up to several hundred km s^{-1}. In Fig. 8, we also see clearly that the case is non-isothermal, and on the downstream side of the shock the temperature is the highest as expected. We note that at $t = 800$ yr, the shock is at ~ 0.3 pc, beyond the scale of UC or compact H II regions. In reality, a champagne shock is so fast that even at a short time-scale of ~ 800 yr the shock is well in the surrounding diffuse interstellar medium (ISM).

Compared with numerical simulations, the advantage of our semi-analytical self-similar approach is clear. We can generate self-similar shock solutions to model different H II regions by varying a few parameters. The self-similar processes and shock solutions of this paper describe the basic hydrodynamics of polytropic 'champagne flows' and serve as test cases for bench marking numerical simulations.
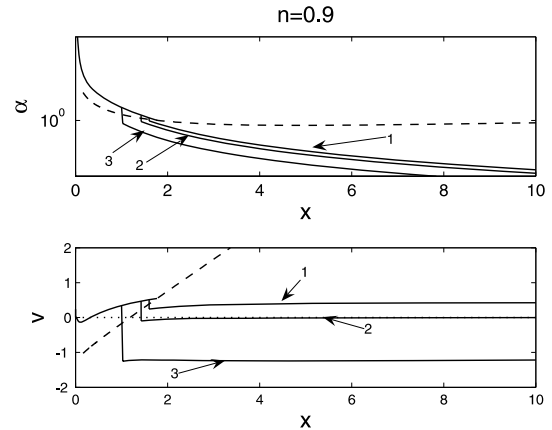
5.2 Asymptotic free-fall solutions around a central protostar

So far we have constructed 'champagne flow' solutions with LP-type asymptotic solutions on the downstream side as $x \to 0^+$, because such asymptotic solution satisfies boundary condition (23). Complementarily, free-fall asymptotic solutions (20) and (21) at $x \to 0^+$ represent gas infall and collapse during the protostar formation phase; and the surrounding gas and the infall momentum
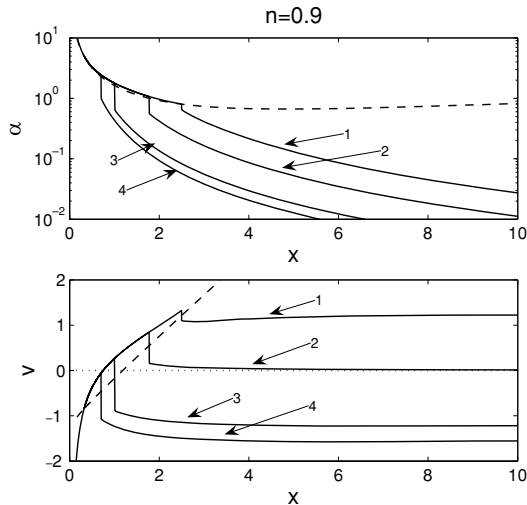
Figure 9. Reduced mass density $\alpha(x)$ (top) and reduced radial flow velocity $v(x)$ (bottom) for global solutions in cases with $n = 0.9$ (thus $\gamma = 1.1$) whose downstream side is free-fall solution and the upstream side corresponds to either outflow, inflow, breeze or contraction. In both panels, the dashed curve represents the sonic critical curve; in the bottom panel the dotted line is $v = 0$. The downstream solution is connected with the upstream solutions with solid curves via shocks. The downstream solution is integrated from a sonic critical point $(x, \alpha, v) = (0.3237, 5.0050, -0.8455)$ towards $x \to 0^+$ with a central free-fall asymptotic solution of $m(0) = 0.546$, and outwards to the downstream shock positions. At the inner most part the downstream solution corresponds to an inflow, and outer part of the downstream side is an outflow. The static point in this case is at $x_{\mathrm{static}} \sim 0.74$. In both panels, the upstream solutions from top to bottom correspond to $x_{\mathrm{sd}} = 2.5$ (labelled 1), 1.7747 (labelled 2), 1 (labelled 3) and 0.7 (labelled 4). Solution 1 has inner inflow and outer outflow on the downstream side and upstream outflow with $A = 4.368$ and $B = 1.76$. The shock parameters are $(x_{\mathrm{sd}}, \alpha_{\mathrm{d}}, v_{\mathrm{d}}) = (2.5, 0.8036, 1.3249)$ and $(x_{\mathrm{su}}, \alpha_{\mathrm{u}}, v_{\mathrm{u}}) = (2.5003, 0.6453, 1.0981)$. Solution 2 has inner inflow and outer outflow on the downstream side and an upstream breeze with $A = 1.8635$ and $B = 0$ at large x. The shock parameters are $(x_{\mathrm{sd}}, \alpha_{\mathrm{d}}, v_{\mathrm{d}}) = (1.7747, 1.0715, 0.8470)$ and $(x_{\mathrm{su}}, \alpha_{\mathrm{u}}, v_{\mathrm{u}}) = (1.7796, 0.5575, 0.1558)$. Solution 3 has an inner inflow and outer outflow on the downstream side and upstream inflow with $A = 0.6930$ and $B = -1.6963$ at large x. The shock parameters are $(x_{\mathrm{sd}}, \alpha_{\mathrm{d}}, v_{\mathrm{d}}) = (1, 1.7883, 0.2668)$ and $(x_{\mathrm{su}}, \alpha_{\mathrm{u}}, v_{\mathrm{u}}) = (1.0118, 0.6348, -0.8942)$. Solution 4 has a downstream inflow and upstream inflow with $A = 0.4899$ and $B = -2.1564$ at large x. The shock parameters are $(x_{\mathrm{sd}}, \alpha_{\mathrm{d}}, v_{\mathrm{d}}) = (0.7, 2.4355, -0.0567)$ and $(x_{\mathrm{su}}, \alpha_{\mathrm{u}}, v_{\mathrm{u}}) = (0.7054, 0.9837, -1.0785)$.

Figure 10. Reduced mass density $\alpha(x)$ (top) and reduced velocity $v(x)$ (bottom) for global solutions in cases of $n = 0.9$ (thus $\gamma = 1.1$) whose downstream side is a free fall and upstream side corresponds to either outflow, inflow, breeze or contraction. In both panels the dashed curve represents the sonic critical curve. The downstream solution is connected with upstream solutions of solid curves via shocks. The downstream solution is integrated from a sonic critical point $(x, \alpha, v) = (1.7727, 1.0050, 0.5463)$ towards $x \to 0^+$ for a free-fall asymptotic solution of $m(0) = 4.638$. Most of the downstream side is an outflow, while the inner most part is a free fall. In both panels, the upstream solutions from top to bottom correspond to $x_{\mathrm{sd}} = 1.6$ (labelled 1), 1.4269 (labelled 2) and 1 (labelled 3). The entire upstream solution labelled 1 has an outflow with $A = 2.8032$ and $B = 0.6058$. Shock parameters are $(x_{\mathrm{sd}}, \alpha_{\mathrm{d}}, v_{\mathrm{d}}) = (1.6, 1.2326, 0.5110)$ and $(x_{\mathrm{su}}, \alpha_{\mathrm{u}}, v_{\mathrm{u}}) = (1.6002, 0.9575, 0.2443)$. Solution labelled 2 has an upstream contraction with $A = 2.115$ and $B = 0$ at large x. Shock parameters are $(x_{\mathrm{sd}}, \alpha_{\mathrm{d}}, v_{\mathrm{d}}) = (1.4269, 1.5391, 0.4705)$ and $(x_{\mathrm{su}}, \alpha_{\mathrm{u}}, v_{\mathrm{u}}) = (1.4290, 0.9057, -0.0988)$. Solution labelled 3 has an inflow for the entire upstream portion with $A = 1.0063$ and $B = -1.6727$. Shock parameters are $(x_{\mathrm{sd}}, \alpha_{\mathrm{d}}, v_{\mathrm{d}}) = (1, 2.9346, 0.3423)$ and $(x_{\mathrm{su}}, \alpha_{\mathrm{u}}, v_{\mathrm{u}}) = (1.0271, 0.7726, -1.2514)$.

associated with the star formation process may be sustained for a while during the evolution after the onset of stellar nuclear burning and UV photoionization of the surrounding gas. Cochran & Ostriker (1977) have investigated consequences of the birth of a massive star within a dense cloud with a free-fall density profile, and found that the radiation pressure from the star sweeps up grains from the infalling gas to form a dust shell which bounds the H II region. Here, we utilize such free-fall solutions as the downstream side and construct global solutions with shocks to model possible dynamic evolutions of H II regions surrounding a nascent protostar in nuclear burning. We present such solutions in Figs 9 and 10 where parameter $m(0)$ for free-fall solutions is different. In dimensionless form, $m(0)$ stands for a central mass point, and with dimensions in self-similar transformation (7), $M(0, t) \propto t^{3n-2} m(0)$; therefore, $m(0)$ scales as the central mass accretion rate. For $m(0) = 0.546$ (Fig. 9), the free-fall solution crosses the sonic critical curve smoothly at $x = 0.3237$, and can also be connected to the upstream solutions

via shocks at various locations. The free-fall solution crosses the line $v = 0$ at $x_{\mathrm{stg}} = 0.74$. This stagnation radius expands with time in a self-similar manner; inside the stagnation radius the gas falls inwards, while outside the stagnation radius the gas expands outwards. Therefore, if $x_{\mathrm{sd}} < x_{\mathrm{stg}}$, the entire global solution corresponds to an inflow (solution 4 of Fig. 9). This situation describes an accretion shock during a protostar formation phase. If $x_{\mathrm{sd}} > x_{\mathrm{stg}}$, the outer part of the downstream side is an outflow. This describes the scenario that the shock sweeps up the gas and turns the gas from infall to expansion on the downstream side near the shock front. Similar to the situation with downstream LP-type solutions, there exists one specific x_{sd}, from which the upstream solution is a breeze with $B = 0$. In this case, $x_{\mathrm{sd}} = 1.7747$ gives an upstream breeze (solution 2 of Fig. 9). Thus for $x_{\mathrm{sd}} < 1.7747$, the upstream side corresponds to an asymptotic inflow far from the centre (solution 3 of Fig. 9) and for $x_{\mathrm{sd}} > 1.7747$, the upstream side corresponds to an asymptotic outflow (wind) far from the centre (solution 1 of Fig. 9). Another example shown in Fig. 10 has $m(0) = 4.638$. This free-fall solution does not cross the sonic critical curve smoothly and can be connected with upstream solutions via shocks. In an analogous manner, we show the possibility to obtain an outflow (solution 1 of Fig. 10), contraction (solution 2 of Fig. 10) and inflow (solution 3 of Fig. 10) for the upstream side. Solutions 1 and 2 of Fig. 9 and solution 1 of Fig. 10 have asymptotic outflow or breeze on the upstream side and in the outer part of the downstream side, which is very similar to champagne flow solutions obtained with a downstream LP type, with different behaviours in central regions. With a

free-fall asymptotic solution, the gravity of the central massive star is not neglected and the gas immediately surrounding the massive protostar still undergoes infall when the outer envelope starts to expand. Hence, solutions with free-fall centre are plausibly suitable to describe the early stage of 'champagne flows'. In general, with central free falls on the downstream side, we can also obtain asymptotic outflow, inflow, breeze and contraction for the upstream side, by varying the downstream shock position x_{sd} in a proper range.

Central free-fall solutions describe the core collapse phase in star formation. For this purpose, Wang & Lou (2008) explored such solutions with free-fall inner core and an inflow or outflow in the outer envelope, for general polytropic cases in their fig. 2. The inner and outer portions are connected by magnetohydrodynamic (MHD) shocks. Such shocks are interpreted as accretion shocks, typically found in a star formation process, or around accreting black holes. Here we specifically emphasize that such shocks may also arise by the UV photoionization of ambient medium surrounding a nascent protostar. Under certain situations, the UV flux from the burning star might not be intense and rapid enough to turn the surrounding gas from infall to expansion by ionization and heating. Meanwhile the IF creates a weak shock travelling outwards, and the upstream side may have an outward velocity. Another possibility is that the gravity of the central star is so large that the gas immediately surrounding the star keeps falling towards the protostar, but the outer part of the downstream side and the corresponding upstream side expand. In summary, with different initial conditions of gas and different physical conditions of a burning protostar, the radiative influence of the nascent protostar on the dynamic evolution of the surrounding gas may give rise to various self-similar solutions, including the classical champagne flow solutions, the ISECE solutions and the inner free fall with outer inflow/outflows or contraction/breeze solutions. The solutions constructed in this paper (classical champagne flows) is suitable for situations that the gas is initially static and the protostar ionizes the entire gas immediately, and then the gas begins to expand in a 'champagne phase' with an outgoing shock.

6 CONCLUSIONS

We present newly established self-similar polytropic shock solutions with and without central voids to model 'champagne flows' in H II regions featuring various asymptotic dynamic behaviours. As a substantial generalization of the isothermal model of Tsai & Hsu (1995) and Shu et al. (2002), we found similarities and differences in self-similar polytropic processes. Our general polytropic 'champagne flow' model allows a much larger freedom to choose the polytropic index $\gamma \geq 1$ for $2/3 < n < 2$; for a conventional polytropic gas as a subclass of examples, the power-law index l of the initial mass density profile $\rho \propto r^{-l}$ is linked to γ by $l = 2/n = 2/(2 - \gamma)$. Together, our model is adaptable to a wide range of initial mass density profile with $1 < l < 3$ for H II regions. For conventional polytropic cases of $1 < \gamma < 4/3$ (i.e. $2/3 < n < 1$ and $2 < l < 3$), we have more freedom for convergent initial conditions. In this fashion, our conventional polytropic shock flow solutions are determined not only by the initial mass density profile (i.e. mass parameter A), but also by the motion at the very early stage (i.e. velocity parameter B). The dimensionless shock positions or the dimensional shock speed and strength are determined by the initial conditions related to A and B and the central density at α_0. Our self-similar shock flow solutions give a plausible description for the 'champagne flow' phase for the dynamics of H II regions. We conclude that general polytropic 'champagne flows' with the initial

density power-law index $1 < l < 3$ may evolve in a self-similar manner.

We have established novel 'champagne flow' shock solutions with an expanding void surrounding the centre to model a certain cloud core whose inner part has fallen into a nascent protostar. We observe that the evolution of central void boundary plays an important role in determining the asymptotic solution to approach and the general behaviour of solutions as well. With even one more free parameter, the 'champagne flow' shock solutions with central voids can model the dynamics of H II regions more realistically, including the effect of central stellar wind bubbles.

We have further explored possibilities of asymptotic inflows or contractions far from the cloud centre. In addition, we also establish global shock solutions with the asymptotic free-fall solution approaching the centre. In general, by varying dimensionless shock position, we connect the downstream side, with either LP-type solutions, EdS solutions or free-fall solutions, to upstream solutions which eventually merge into asymptotic outflow, breeze, contraction and inflow. Within the theoretical framework of the self-similar polytropic fluid, global shock solutions with different behaviours correspond to different forms of hydrodynamic evolution of H II regions after the nascence of a central massive protostar. Apparently, even within the framework of self-similarity, dynamic evolution of polytropic H II regions depends on the initial and boundary conditions of molecular clouds. Numerical simulations are needed to probe and connect various self-similar evolution phases.

Finally, we note that our work is also an extension of the isothermal model analysis by Chevalier (1997) as applied to the dynamics of planetary nebulae. Our model involves a polytropic equation of state and the gas self-gravity. In this context, the void boundary obeying the relation $nx - v = 0$ is a surface of contact discontinuity sandwiched between the outer slower wind and the inner faster wind whose mass is negligible. The self-similar isothermal model of Chevalier (1997) corresponds to $n = 1$ here. The polytropic shocks shown in our global solutions are physically created by the persistent driving of inner faster winds. Even within the isothermal model framework, we can also accommodate two different constant temperatures across an outgoing shock (e.g. Shen & Lou 2004; Bian & Lou 2005).

REFERENCES

Arquilla R., Goldsmith P. F., 1985, ApJ, 297, 436
Arthur S. J., Hoare M. G., 2006, ApJS, 165, 283
Barriault L., Joncas G., 2007, ApJ, 667, 257
Bian F. Y., Lou Y.-Q., 2005, MNRAS, 363, 1315
Bodenheimer P., Sweigart A., 1968, ApJ, 152, 515
Bodenheimer P., Tenorio-Tagle G., Yorke H. W., 1979, ApJ, 233, 85
Cheng A. F., 1978, ApJ, 221, 320
Chevalier R. A., 1997, ApJ, 488, 263
Cochran W. D., Ostriker J. P., 1977, ApJ, 211, 392

Comerón F., 1997, A&A, 326, 1195

De Buizer J. M., Radomski J. T., Piña R. K., Telesco C. M., 2002, ApJ, 580, 305

Fatuzzo M., Adams F. C., Myers P. C., 2004, ApJ, 615, 813

Fish M., 1993, ApJS, 86, 475

Foster T. J., Kothes R., Kerton C. R., Arvidsson K., 2007, ApJ, 667, 248

Franco J., Tenorio-Tagle G., Bodenheimer P., 1990, ApJ, 349, 126

Franco J., Kurtz S., Hofner P., Testi L., García-Segura G., Martos M., 2000, ApJ, 542, L143

Galli D., Lizano S., Li Z. Y., Adams F. C., Shu F. H., 1999, ApJ, 521, 630

Goldreich P., Weber S. V., 1980, ApJ, 238, 991

Habing H. J., Israel F. P., ARA&A, 17, 345

Hunter C., 1977, ApJ, 218, 834

Kurtz S., Churchwell E., Wood D. O. S., 1994, ApJS, 91, 659

Larson R. B., 1969a, MNRAS, 145, 271

Larson R. B., 1969b, MNRAS, 145, 405

Lou Y.-Q., Cao Y., 2008, MNRAS, 384, 611

Lou Y.-Q., Gao Y., 2006, MNRAS, 372, 1610

Lou Y.-Q., Hu R.-Y., 2008, MNRAS, submitted

Lou Y.-Q., Wang W.-G., 2006, MNRAS, 372, 885

Lou Y.-Q., Jiang Y. F., Jin C. C., 2008, MNRAS, 386, 835

Lumsden S. L., Hoare M. G., 1999, MNRAS, 305, 701

McLaughlin D. E., Pudritz R. E., 1997, ApJ, 476, 750

Maheswar G., Sharma S., Biman J. M., Pandey A. K., Bhatt H. C., 2007, MNRAS, 379, 1237

Myers P. C., 1985, Protostars and Planets. University of Arizona Press, Tucson

Osterbrock D. E., 1989, Astrophysics of Gaseous Nebulae and Active Galactic Nuclei. University Science Books, Mill Valley, CA

Penston M. V., 1969a, MNRAS, 144, 425

Penston M. V., 1969b, MNRAS, 145, 457

Shen Y., Lou Y.-Q., 2004, ApJ, 611, L117

Shu F. H., 1977, ApJ, 214, 488

Shu F. H., Lizano S., Galli D., Cantó J., Laughlin G., 2002, ApJ, 580, 969

Suto Y., Silk J., 1988, ApJ, 326, 527

Tenorio-Tagle G., 1979, A&A, 71, 59

Tenorio-Tagle G., Yorke H. W., Bodenheimer P., 1979, A&A, 80, 110

Tenorio-Tagle G., Bodenheimer P., Lin D. N. C., Noriega-Crespo A., 1986, MNRAS, 221, 635

Tsai J. C., Hsu J. J. L., 1995, ApJ, 448, 774

Wang W.-G., Lou Y.-Q., 2008, ApSS, 353, 249

Wood D. O. S., Churchwell E., 1989, ApJS, 69, 831

Yorke H. W., 1986, ARA&A, 24, 49

APPENDIX A: AN INVARIANT FORM

Transformation (7) leads to an initial density profile $\rho \propto r^{-2/n}$ as the outer part of a SPS. To model an initial mass density profile other than a SIS (e.g. Galli et al. 1999) in the self-similarity framework, Shu et al. (2002) developed an invariant self-similar transformation for an isothermal gas by neglecting the self-gravity. We extend below this invariant transformation to a conventional polytropic gas.

The independent similarity variable is $x = r/(k^{1/2}t^n)$ and the reduced radial velocity $v(x)$ still reads as $v = u/(k^{1/2}t^{n-1})$. However, the mass density ρ is generalized to

$$\rho(r, t) = \frac{D}{r^l} R(x), \qquad (A1)$$

where $R(x)$ is a new reduced density dependent on x only, l is a scaling index and D is a constant parameter to be determined. With the conventional polytropic relation $p = \kappa \rho^\gamma$ for constant κ and γ, the thermal pressure p is

$$p(r, t) = \kappa \frac{D^\gamma}{r^{\gamma l}} R^\gamma. \qquad (A2)$$

We now determine the relation between k and κ from the radial momentum equation without self-gravity:

$$\frac{\partial u}{\partial t} + u \frac{\partial u}{\partial r} = -\frac{1}{\rho} \frac{\partial p}{\partial r}. \qquad (A3)$$

The left-hand side (LHS) of equation (A3) relates to the sound scaling parameter k and the right-hand side (RHS) relates to the specific entropy coefficient κ. We substitute self-similar transformation (A1) and (A2) into both sides of the radial momentum equation (A3) to obtain

$$\frac{\partial u}{\partial t} + u \frac{\partial u}{\partial r} = k^{1/2}t^{n-2}[(n-1)v + (v - nx)v'], \qquad (A4)$$

$$-\frac{1}{\rho} \frac{\partial p}{\partial r} = -\kappa D^{\gamma-1}\gamma(k^{-1/2}t^{-n})^{(\gamma-1)l+1}x^{-(\gamma-1)l}$$
$$\times \left(-\frac{l}{x}R^{\gamma-1} + R'R^{\gamma-2}\right), \qquad (A5)$$

where the superscript '′' over $v(x)$ and $R(x)$ indicates the first derivative in x. By expressions (A4) and (A5) and in order to remove the explicit t dependence in the self-similar form of equation (A3), we require

$$-n[(\gamma-1)l + 1] = n - 2. \qquad (A6)$$

Together with $n + \gamma = 2$ for a conventional polytropic gas, we obtain $l = 2/n$ for $n \neq 1$. For $n = 1$, there is no constraint on l. For a conventional polytropic gas, the possible initial mass density profile described by this invariant self-similar transformation is not arbitrary, but is pre-set by the scaling index n or by the polytropic index γ. Here D provides a measure for the magnitude of density profile and κ is the constant in the polytropic equation of state; both parameters are determined physically. For simplicity of the formulation, we may choose the sound parameter k so that

$$\kappa = k^{1/n}D^{n-1}. \qquad (A7)$$

This relation is verified by a dimensional analysis. As a result, these parameters disappear in the following ODEs:

$$[(nx - v)^2 - \gamma x^{2-l}R^{\gamma-1}]R'$$
$$= \frac{Rv}{x}[(l-2)(v-nx) + (n-1)x] - \gamma l x^{1-l}R^\gamma, \qquad (A8)$$

$$[(nx - v)^2 - \gamma x^{2-l}R^{\gamma-1}]v'$$
$$= 2\gamma x^{1-l}R^{\gamma-1}(v-x) + (n-1)v(nx-v). \qquad (A9)$$

For $n \neq 1$ and $l = 2/n$, coupled equations (A8) and (A9) describe non-isothermal self-similar flows of a conventional polytropic gas. For $n = 1$ and $\gamma = 1$, the value of l is arbitrary; for $l = 2$, these two coupled non-linear ODEs reduce to the isothermal formulation of Shu et al. (2002) with two decoupled ODEs for $l = 2$. For $n = 1$ and $\gamma = 1$ with $l \neq 2$, we need to use the two decoupled ODEs (32) and (33) in section 4 of Shu et al. (2002). In contrast to the isothermal case, the non-linear ODEs here remain coupled for $\gamma \neq 1$. In summary, with our self-similar transformation, hydrodynamics for a spherical gas with ignorable gravity can be expressed by a set of two coupled non-linear ODEs (A8) and (A9).

In cases with $\gamma \neq 1$ and for $x \to +\infty$, the asymptotic boundary conditions are $v \to 0$ and $R \to 1$ for $n < 1$. The asymptotic solution at large x yields

$$v = Hx^{1-1/n} + \frac{2\gamma}{n}x^{1-2/n} + \cdots,$$

$$R = 1 + 3H\left(\frac{1}{n} - 1\right)x^{-1/n} + \cdots, \qquad x \to +\infty, \qquad (A10)$$

where H is an arbitrary constant but should be chosen for a positive mass density everywhere. The condition $l = 2/n$ has already been taken into account in this solution. This form of asymptotic solution at large x differs from equation (34) of Shu et al. (2002), because for non-isothermal cases the leading terms in non-linear ODEs (A8) and (A9) are different; however, the second term on the RHS of the expression of v, reduces to the v expression in equation (34) of Shu et al. (2002) for $n = 1$ and $\gamma = 1$. The form (A10) is similar to the form of (18) and (19) in the overall scaling. The integration constant H in the invariant form is an analogy of the 'velocity parameter' B, while the 'mass parameter' A is already absorbed into the parameter D in the invariant form. To make this asymptotic solution applicable, we should require $H = 0$ in cases of $n < 1$ and thus $\gamma > 1$. The boundary conditions at $x \to +\infty$ correspond to the initial conditions of the fluid. Therefore, the initial density scales as r^{-l}. More precisely, this new self-similar transformation requires the initial density profile to scale as $r^{-2/n}$, identical with the scaling we obtain in the main text using self-similar transformation (7). For $x \to 0^+$, the asymptotic solution reads

$$v \sim 2x/3, \qquad R \sim I x^l, \qquad \text{as} \quad x \to 0^+, \qquad \text{(A11)}$$

where $I > 0$ is an arbitrary parameter for a positive mass density. This v expression of asymptotic solution (A11) is independent of l, different from the v expression (35) in Shu et al. (2002), but it is similar to asymptotic solution (24) in the main text; the R expression of our asymptotic solution is similar to the R expression (35) of Shu et al. (2002), and the parameter I here is proportional to the central reduced mass density α_0. In the isothermal case with $n = 1$ and $\gamma = 1$, relation (A6) is satisfied automatically and parameter l is thus arbitrary. Here lies a fundamental difference between the conventional polytropic case and the isothermal case.

This paper has been typeset from a TeX/LaTeX file prepared by the author.